NASA TECHNICAL NOTE

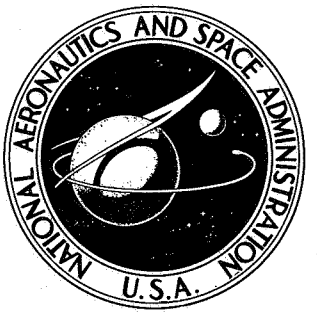

NASA TN D-5929

NASA TN D-5929

BLOCK AND STRIP SOLUTIONS INVOLVING LUNAR ORBITER PHOTOGRAPHIC DATA USED TO PREPARE CONTOUR CHARTS FOR FIVE APOLLO LANDING SITES

by Ruben L. Jones

Langley Research Center
Hampton, Va. 23365

NATIONAL AERONAUTICS AND SPACE ADMINISTRATION • WASHINGTON, D. C. • AUGUST 1970

1. Report No.	2. Government Accession No.	3. Recipient's Catalog No.
NASA TN D-5929		

4. Title and Subtitle	5. Report Date
BLOCK AND STRIP SOLUTIONS INVOLVING LUNAR ORBITER PHOTOGRAPHIC DATA USED TO PREPARE CONTOUR CHARTS FOR FIVE APOLLO LANDING SITES	August 1970
	6. Performing Organization Code
7. Author(s)	8. Performing Organization Report No.
Ruben L. Jones	L-6981
	10. Work Unit No.
9. Performing Organization Name and Address	185-42-12-01
NASA Langley Research Center Hampton, Va. 23365	11. Contract or Grant No.
	13. Type of Report and Period Covered
12. Sponsoring Agency Name and Address	Technical Note
National Aeronautics and Space Administration Washington, D.C. 20546	14. Sponsoring Agency Code

15. Supplementary Notes

16. Abstract

The selenographic coordinates of many distinct lunar features in the vicinity of Sinus Medii were calculated with an estimated uncertainty in the absolute position of ±1 km by a digital computer program using film readings from eight sequences (strips) of Lunar Orbiter photographs which contained common lunar terrain. The film readings from three strips of photographs exposed from three consecutive orbits during the second Lunar Orbiter mission were processed both separately (a "strip" solution) and in various combinations ("block" solutions). A comparison of the selenographic coordinates resulting from the various block and strip solutions revealed that a block solution involving data from consecutive orbits computed from a common data arc was the preferred solution. Also, a comparison of the results of block solutions involving data from different missions and different data arcs revealed significant biases to exist in either latitude or longitude. In all cases studied, the lunar radii were found to compare favorably. As a result of this study, the selenographic coordinates of lunar features were calculated from film readings on mission II film for each of the five original Apollo landing sites and the results are portrayed in contour charts.

17. Key Words (Suggested by Author(s))	18. Distribution Statement
Lunar Orbiter photographic data Selenodesy Photographic analysis Selenographic coordinates Lunar radii	Unclassified – Unlimited

19. Security Classif. (of this report)	20. Security Classif. (of this page)	21. No. of Pages	22. Price*
Unclassified	Unclassified	68	$3.00

*For sale by the Clearinghouse for Federal Scientific and Technical Information
Springfield, Virginia 22151

BLOCK AND STRIP SOLUTIONS INVOLVING LUNAR ORBITER PHOTOGRAPHIC DATA USED TO PREPARE CONTOUR CHARTS FOR FIVE APOLLO LANDING SITES

By Ruben L. Jones
Langley Research Center

SUMMARY

A study of the Lunar Orbiter photographs is being conducted which, when complete, should yield a very good estimate of the lunar size and shape and contribute significantly to the establishment of an accurate selenodetic system. This paper is a report on results obtained from a comparison of the selenographic coordinates resulting from strip and block solutions involving film readings of features on photographs exposed in the vicinity of Sinus Medii.

The selenographic coordinates of many distinct lunar features in the vicinity of Sinus Medii were calculated with an estimated uncertainty in the absolute position of ±1 km by a digital computer program using film readings from eight sequences (strips) of Lunar Orbiter photographs which contained common lunar terrain. The film readings from three strips of photographs exposed from three consecutive orbits during the second Lunar Orbiter mission were processed both separately (a "strip" solution) and in various combinations ("block" solutions). A comparison of the selenographic coordinates resulting from the various block and strip solutions revealed that a block solution involving data from consecutive orbits computed from a common data arc was the preferred solution. Also, a comparison of the results of block solutions involving data from different missions and different data arcs revealed significant biases to exist in either latitude or longitude. In all cases studied, the lunar radii were found to compare favorably.

As a result of this study, the selenographic coordinates of lunar features were calculated from film readings on mission II film for each of the five original Apollo landing sites and the results are portrayed in contour charts.

INTRODUCTION

As pointed out in reference 1, the Lunar Orbiter series of spacecraft photographed approximately 99 percent of the moon's surface, for the first time, with both high and moderate resolution cameras at altitudes ranging from 50 to approximately 2000 km.

Most of the photographs were taken in sequences of overlapping photographs exposed during one orbital pass. In some instances, sites were rephotographed on consecutive orbital passes, consecutive missions, or both. Thus, sidelapping sequences of overlapping photographs were obtained. These sequences can be utilized to determine the approximate uncertainty to be expected in the absolute selenographic coordinates which result from an analytical stereoscopic analysis of film readings on the images of photographed lunar features. Also, a comparison of results involving data from various single sequences (strip solutions) and of results involving various combinations of data from different photographic sequences (block solutions) can be utilized to determine which of the two techniques yields the most consistent results.

In references 2, 3, and 4, the accuracy of photographic site location resulting from uncertainties in spacecraft orbital predictions and uncertainties in times of exposure for each photograph were investigated. From these references an improved set of photographic support data for each of the five Lunar Orbiter missions was determined.

The present paper and reference 1 are the initial reports on a continuing study of the moon's size and shape, utilizing the Lunar Orbiter photographs from mission I. In reference 1, the concepts for performing the analytical stereoscopic analysis, the procedures established for reading the film from the first Lunar Orbiter mission, and some of the preliminary results obtained from mission I photography were presented. The first objective of this paper is to investigate, by using the updated photographic support data, those optimum conditions under which the film readings from the photographs exposed from different orbital passes and/or missions can be introduced into the same solution (termed a "block" solution) to obtain one set of coordinates for each feature that will best represent the data from all exposures. Secondly, the discrepancies in the coordinates of the lunar features resulting from different orbits, data arcs, and missions utilizing several hundred points nominally distributed over the site or sites are investigated. Finally, preliminary contour charts for the five original primary Apollo landing sites are presented by using the findings from the first two objectives.

This paper utilizes techniques discussed in reference 1 with certain improvements in the preprocessing and processing of film readings. Each improvement is briefly discussed.

SYMBOLS

A	matrix of coefficients of equation of condition in $\mathbf{X}$
a,b	photographic coordinates of an image

B	magnitude of base line
C	matrix of coefficients of equation of condition in Y
D	matrix of coefficients of equation of condition in Q
E	matrix of residuals
f	camera focal length
H	height of camera above feature
l	number of photographs in a sequence
n	number of features identified
P	lunar feature
Q,S,W	functions of camera attitude, focal length, and height
R	magnitude of radius vector to spacecraft
r	magnitude of selenocentric radius to feature
s	number of sequences
w	assigned weight
X,Y,Z	axes of moon-centered rectangular Cartesian coordinate system with the Z-axis parallel to the datum radius vector, the Y-axis in the direction of spacecraft motion, and the X-axis completing the right-handed system. The Y,Z plane is the plane of the orbit
x,y,z	rectangular coordinates of a point
Δ	a small difference between two variables or two vectors
δ	an incremental change in a variable

ϵ	residual
θ	swing component of camera attitude
ρ	line of projection of feature image through camera lens
σ	standard deviation
Φ	selenographic latitude
φ	roll component of camera attitude
λ	selenographic longitude
τ	tilt component of camera attitude

Subscripts:

g	a particular value of a multivalued incremented variable
i	a particular lunar feature
j	a particular reference photograph or vector (j = 1, 2, . . .)
k	a particular reference photograph or vector (k = 1, 2, . . .)
l,m	integers implying different solutions to a particular variable
n	intermediate reference photograph or vector
o	datum reference system, photograph, vector, or variable
x,y,z	components of a variable
q,s,w	used to denote the particular function or condition for a residual
u,v	used to denote the particular sequence to which the subscripts j and k refer

Matrix exponents:

T	indicates the transpose
-1	indicates the inverse

Notation:

$\{\ \}$	column matrix
$[\ ]$	square matrix
$\| \ \|$	rectangular matrix
*	least-squares estimate

A bar over a symbol indicates a vector. A bar below a symbol indicates an approximation. A prime indicates a transformed variable. Missions are denoted by Roman numerals, sites by Arabic numbers, and photographic sequences by A,B,C,. . . . For example: II P-8 denotes mission II, primary site 8; II P-8A denotes strip solution for photographic sequence II P-8A within the II P-8 area; III P-7AB denotes block solution for photographic sequences III P-7A and III P-7B.

DEFINITION OF PROBLEMS

Photographic Support Data

In references 2, 3, and 4, an error analysis for representative photographic frames from the five Lunar Orbiter missions is reported. In the references, selenographic latitude and longitude errors were determined for the camera axis intercept, for the corner points of each frame, and for those points approximately midway between each corner (nine points) for selected photographs. These points were found to be common to photographs from other missions; thus, it was possible to isolate the sources of error in the photographic support data.

In brief, it was found that the total error in latitude and longitude of each point was a result of the combined effect of errors in navigation, camera attitude, camera-on time, and moon radius. (Since film readings from single photographs were utilized to compute latitudes and longitudes, it was necessary to assume a mean lunar radius. Thus, an

uncertainty in the assumed mean lunar radius contributed to the total uncertainty in the location of each point.) The uncertainties were generally found to be smaller for those points on the photograph which were closest to the spacecraft radius vector and larger for those points which were farthest away. For those frames selected from missions I, II, III, and V (referred to as Apollo frames), the typical errors were found to be less than 0.6 km in latitude and longitude for the moderate resolution camera. In some cases, errors of a few kilometers or more were found to exist. In general, it was found that for missions I, II, III, and V frames at low altitudes (46 to 240 km), the total photographic error variance is a combination of significant contributions from attitude and navigation sources, a significant contribution for some frame points being due to moon radius error, especially for the moderate resolution camera. For the altitudes greater than 240 km, the attitude error was the predominant contributor. Further, errors of a few kilometers were not uncommon in missions I, II, III, and V. Finally, it was determined that the photographic errors due to uncertainties in a revised set of camera-on times were essentially negligible for all frames. (See ref. 2.)

The analysis was a thorough one and resulted in a complete set of revised photographic support data. (See refs. 5 to 9.) These photographic support data represent the very best results available and are now being used exclusively in this study. Uncertainties in absolute spacecraft position of 1 km and attitude uncertainties on the order of 0.1^{o} are to be expected, except in those cases where attitude uncertainties could be larger because of large attitude maneuvers.

The photographic support data for each photograph in a sequence of photographs were computed from those real-time attitude maneuver commands given to the spacecraft prior to photographing a lunar site and the spacecraft state at the time each photograph was exposed. The spacecraft state for each photograph in a sequence was determined from a common data arc. Thus, an uncertainty in the absolute position of the spacecraft is a result of orbital uncertainties and applies equally to all radius vectors determined from a common data arc. Uncertainties in the relative positions of the spacecraft are not affected by the absolute uncertainty in position since the absolute uncertainty applies equally to all radius vectors resulting from a common data arc.

Relative Merits of Strip and Block Solutions

The digital computer program utilized in the present study assumes the photographs of each photographic sequence to be constrained to that orbit defined by the photographic support data and solves for that camera attitude which will minimize the discrepancies in the selenographic coordinates of all the features as determined from all the photographs for which each feature is common. As was shown in reference 1, uncertainty in the relative spacecraft positions will affect first the base vectors and then the resulting camera

attitude whereas an uncertainty in the absolute spacecraft position will not affect the camera attitude, since the base vector is not disturbed by absolute positional uncertainties. In those cases where it becomes necessary to process data obtained from different data arcs, the effect of an absolute uncertainty must then be considered to be the same as that of a relative uncertainty.

During the course of this study, numerous sequences of photographs from Lunar Orbiter missions I, II, and III have been studied. In the process, numerous lunar features were selected from each site and given an identification number. Furthermore, a particular feature maintained its numerical identity when rephotographed from an adjacent orbital pass or a later mission. Thus, it would be desirable to combine the film measurements observed on sidelapping photographs exposed from adjacent orbital passes, from different missions, and so forth, into one solution to obtain a consistent set of estimated selenographic coordinates for all features identified on the sidelapping photographic sequences.

Either block or strip solutions can be used to achieve the stated goal of combining film readings from several photographic sequences into one set of consistent selenographic coordinates. Each approach has both advantages and disadvantages. A block solution, although subject to relative cross-orbital uncertainties, will yield results which are internally consistent over the whole terrain photographed from all orbital passes considered. Strip solutions, however, will yield results which are internally consistent within themselves, discrepancies existing between the coordinates of features which are common to different strips. These discrepancies are the result of a combination of the relative cross-orbital uncertainty and of an incomplete solution to the camera attitude. (In strip solutions, the roll component of camera attitude must be either known or assumed to be 0^{o}.) Thus, to obtain a set of results which would apply with equal certainty to the whole terrain encompassed by several photographic strips would require that all the results from each of the strip solutions be corrected simultaneously by some form of feature matching or other innovation.

Consider figure 1 in which photographs covering the same site and taken from two different orbits are depicted. In the figure, it is shown that six base vectors are possible. As a result, 18 condition equations can be written for the block solution involving the 4 photographs which contain the common point P whereas only 3 condition equations can be written for each strip solution (a total of 6 condition equations). Therefore, it should be possible to obtain a better solution for the selenographic coordinates of the feature P from a block solution, provided the uncertainties in orbit do not significantly reduce the accuracy of the estimated camera attitude angles. Since the technique utilized in this study will not permit that component of the camera attitude normal to the orbital plane to be determined in strip solutions, the block solution permits a more complete solution of the camera attitude. However, a block solution involving photographic data from different

missions and different data arcs must be rejected since the absolute uncertainty in the spacecraft position will affect the estimated camera attitude.

Statement of Objectives

From the foregoing discussion, it is evident that a block solution possesses many advantages and data from two or more sequences of photographs is a more desirable solution than the appropriate strip solutions involving the same data. However, it is necessary to determine whether relative cross-orbital uncertainties will significantly affect the results.

In no case where a given site was photographed from two or more consecutive orbits during the same mission were the spacecraft states computed from differing data arcs. Also, there was no extrapolation beyond the data arc. Thus, a comparison of results from block and strip solutions involving the same film data should permit that solution yielding the best results to be selected. To achieve this goal, those sequences of photography obtained in the vicinity of Sinus Medii were utilized since this region was photographed from different missions and from two different sets of consecutive orbital passes. These sequences have been identified as follows: from mission I, I P-5; from mission II, II P-8A, II P-8B, and II P-8C (one data arc) and II P-7A and II P-7B (a second data arc) and from mission III, III P-7A and III P-7B. Both of the adjoining sites II P-7A and II P-7B and II P-8A, II P-8B, and II P-8C contain lunar terrain which is common to sites III P-7A and III P-7B (a result of the higher orbital inclination of mission III). In figure 2, the approximate positions of the various sites relative to each other are plotted and in table I the number of features identified on each sequence are tabulated along with the number of features common to and existing between the various strip and block solutions studied. As can be seen from the table, in certain cases the number of points common to different solutions is large whereas in other cases the number of points common to different solutions is small.

COMPUTATIONAL TECHNIQUES AND DATA PREPARATION

Refinements in Data Processing

Figure 3 shows the vector relations existing when the images of a lunar feature on two photographs exposed from an orbiting spacecraft are projected through the lens of the camera to the feature on the lunar surface (the vectors $\overline{\rho}_{i,j}$ and $\overline{\rho}_{i,k}$). In the figure, the spacecraft radius vectors $\overline{R}_k$ and $\overline{R}_j$ are assumed to be known and lie in the plane of the paper. Thus, the base vector $\overline{B}_{j,k}$ is determined by the vector sum

$$\overline{B}_{j,k} = \overline{R}_k - \overline{R}_j$$

Further, it is seen that the base vector can also be expressed as

$$\overline{B}_{j,k} = \overline{\rho}_{i,j} - \overline{\Delta} - \overline{\rho}_{i,k}$$

where the ρ and Δ vectors are generally not coplanar and their differences $\overline{\Delta}$ will have a nonvanishing component normal to a plane defined by the product $\left(\overline{\rho}_{i,j} \times \overline{\rho}_{i,k}\right)$ because of uncertainties in the camera attitude, and so forth.

In reference 1, analytical expressions were derived relating the individual x, y, and z components of the ρ-vectors to the calibrated camera focal length f, measured photographic coordinates of the images $a_{i,j}$, $b_{i,j}$, $a_{i,k}$, and $b_{i,k}$, and the camera attitude angles θ_j, φ_j, τ_j, θ_k, φ_k, and τ_k. As a result, it was determined that

$$\rho_{x,i,j} - \rho_{x,i,k} = W_{i,j,k}\left(f,a_{i,j},a_{i,k},b_{i,j},b_{i,k},\varphi_j,\varphi_k,\theta_j,\theta_k,\tau_j,\tau_k,H_{o,i},B_{z,o,j},B_{z,o,k}\right)$$

$$\rho_{y,i,j} - \rho_{y,i,k} = S_{i,j,k}\left(f,a_{i,j},a_{i,k},b_{i,j},b_{i,k},\varphi_j,\varphi_k,\theta_j,\theta_k,\tau_j,\tau_k,H_{o,i},B_{z,o,j},B_{z,o,k}\right)$$

where

$$H_{o,i} = T_{i,j,n}\left(f,a_{i,j},a_{i,n},b_{i,j},b_{i,n},\theta_j,\theta_n,\varphi_j,\varphi_n,\tau_j,\tau_n,B_{z,o,j},B_{z,o,n},B_{y,j,n}\right)$$

is the height of the camera reference position above the feature. In the event a single sequence or strip of photographs,

$$\theta_j = \theta_k = \theta_n$$

$$\varphi_j = \varphi_k = \varphi_n$$

$$\tau_j = \tau_k = \tau_n$$

and the subscripts can be dropped from the attitude angles since they are considered to be constant. Thus, the least-squares condition necessary to minimize the two components of $\overline{\Delta}$ was found to be

$$\sum_{i}^{n}\sum_{j}^{l}\sum_{k}^{l}\left(\epsilon_{w,i,j,k}^2 + \epsilon_{s,i,j,k}^2\right) = \text{Minimum} \qquad (1)$$

where

$$\epsilon_{w,i,j,k} = B_{x,j,k} - \underline{W}_{i,j,k}$$

$$\epsilon_{s,i,j,k} = B_{y,j,k} - \underline{S}_{i,j,k}$$

where the bars beneath W and S imply that they are approximated.

The iterative technique for minimizing $\overline{\Delta}$ as discussed in reference 1 is wholly adequate and correct. However, convergence was slow. As a result, a condition which tends to make each pair of ρ-vectors coplanar and their extensions intersect and which will aid the convergence by directing the search toward solutions which do converge was needed. Thus, from figure 1, it can be seen that

$$\left(\overline{\rho}_{i,j} \times \overline{\rho}_{i,k}\right) \cdot \overline{\Delta} = \left(\overline{\rho}_{i,j} \times \overline{\rho}_{i,k}\right) \cdot \left[\left(\overline{R}_j + \overline{\rho}_{i,j}\right) - \left(\overline{R}_k + \overline{\rho}_{i,k}\right)\right] = Q\left(\overline{\rho}_{i,j}, \overline{\rho}_{i,k}, \overline{R}_j, \overline{R}_k\right) = \text{Minimum} \tag{2}$$

satisfies the requirement. Upon linearization,

$$Q = \underline{Q} + Q'$$

or

$$\epsilon_{q,i,j,k} = Q - \underline{Q} = Q'$$

where $\epsilon_{q,i,j,k}$ represents the residual, $\underline{Q}$ is an approximate value of Q, and Q' is the function of the partial derivatives of Q with respect to the camera attitude resulting from the expansion of Q.

In the present paper equation (1) is modified so that

$$\sum_{i}^{n} \sum_{j}^{l} \sum_{k}^{l} \left(\epsilon^2_{w,i,j,k} + \epsilon^2_{s,i,j,k} + \epsilon^2_{q,i,j,k}\right) = \text{Minimum} \tag{3}$$

The partial differentiation of Q with respect to $\rho_{i,j}$ and $\rho_{i,k}$ is given in appendix A. (See reference 1 for the partials of $\rho_{i,j}$ and $\rho_{i,k}$ with respect to the camera attitude.)

Equations (1) to (3), as written, are adequate when strip solutions are being considered. However, in the event of block solutions, j and k can represent photographs from different sequences and should be subscripted. Since summations must now be taken over differing sequences, equation (1) is rewritten as

$$\sum_{i=1}^{n}\sum_{u=1}^{s}\sum_{v=1}^{s}\sum_{j_u}^{l_u}\sum_{k_v}^{l_v}\left(\epsilon^2_{w,i,j_u,k_v}+\epsilon^2_{s,i,j_u,k_v}+\epsilon^2_{q,i,j_u,k_v}\right)=\text{Minimum} \tag{4}$$

Thus, the least-squares solution in reference 1 becomes

$$\begin{Bmatrix}\Delta\theta_1\\ \Delta\tau_1\\ \Delta\varphi_1\\ \vdots\\ \Delta\theta_s\\ \Delta\tau_s\\ \Delta\varphi_s\end{Bmatrix}^{*}=\left[\left[\|A\|^T\|A\|\right]+\left[\|C\|^T\|C\|\right]+\left[\|D\|^T\|D\|\right]\right]^{-1}\left[\|A\|^T\{E_w\}+\|C\|^T\{E_s\}+\|D\|^T\{E_q\}\right] \tag{5}$$

where A, C, and D represent $ns^2l_vl_u \times 3$ weighted matrices of partial derivatives resulting from the W, S, and Q conditions, respectively, and E_w, E_s, and E_q are the corresponding matrices of residuals.

Upon careful analysis, no change in the selenographic coordinates of features was noted as a result of adding the Q condition. In fact, the only effect was to insure a more rapid convergence of the differential corrections to the estimated attitude of the camera (6 iterations as opposed to 20 iterations).

Weighting Function

Each condition, as in reference 1, was weighted by the empirically derived expression

$$w^2_{i,j_u,k_v}=\left(\frac{f^2}{f^2+a^2_{i,j_u}+b^2_{i,j_u}}+\frac{f^2}{f^2+a^2_{i,k_v}+b^2_{i,k_v}}\right)\frac{\left|B_{y,j_u,k_v}\right|}{H_{o,i}} \tag{6}$$

where B_{y,j_u,k_v} replaces $B_{j,k}$. In reference 1, since only those solutions involving single sites or sequences were emphasized, it was not necessary to make the distinction between the magnitude of the base vector and its Y component. In the present paper, however, both block and strip solutions are considered.

In the case of a block solution, it is conceivable that observations will be obtained from photographs with a small Y-component of base (downrange component). Relative cross-orbital uncertainties will then tend to be a more significant component of the total base vector when B_{y,j_u,k_v} is small than when it is large. Since the weighting function (eq. (6)) is dependent on the Y-component of the base, those cross-orbital condition equations involving photographs whose Y-component of the base is nearly zero will be essentially weighted out of the matrix of observations. Thus, the effect of cross-orbital uncertainties on estimated attitude angles should be significantly reduced by equation (6).

Data Preparation

The analysis of mission I photography (edge data and test patterns) revealed nonlinearities in the spacecraft photosubsystem optical-mechanical scanner. To assist in compensating for this nonlinearity, reseaux (a term used in various contractor reports to describe the preprinted geometric pattern of crosses) were pre-exposed on the spacecraft film at regular intervals across its width (ref. 10) for subsequent flights.

For missions III, IV, and V, the pre-exposed reseaux were staggered to appear as is shown in figure 4. In so doing, those nonlinearities in the optical-electrical scan direction (see fig. 4) could be compensated for. In each case, the reseau patterns were carefully calibrated and appear at the same location relative to the gray scale for each gray scale number. As a result, each reseau on the film was read along with other preprinted data and sawteeth.

Since the relative positions of the reseaux have been carefully determined from thousands of measurements by different observers on samples of the spacecraft film, the orientation of the framelet relative to the comparator X-axis (along the optical-mechanical scan direction) (see fig. 4) is computed mathematically by the technique of least squares from differences between the measured relative positions of each of the reseaux contained in the framelet and their corresponding relative calibrated positions.

In addition to being a useful tool for determining framelet orientation relative to the comparator X-axis, the preprinted patterns may also be used to determine the scale for reducing comparator measurements to the spacecraft equivalent by simply determining the ratio of the calibrated coordinates of the various reseaux to the corresponding measured coordinates. The scale was re-evaluated for each framelet, and upon examination, was found to have an accuracy of 0.0004.

The reassembly of the spacecraft frame from comparator measurements is accomplished in the same fashion as in reference 1; that is, x- and y-coordinates of a feature relative to its reseaux can be converted into x- and y-coordinates relative to the gray scale nearest to the principal point of the photograph by using the gray scale number associated with each framelet (see fig. 4) as a means for counting the number of reseau patterns (cycles) between the feature and the gray scale of that framelet containing the principal point. Since the principal point was calibrated relative to each sawtooth (there are 84 sawteeth on each moderate resolution photograph) that gray scale containing the principal point and its coordinates relative to the gray scale are determined analytically for each photograph from the sawteeth measurements. Thus, the measurements for each feature, for each reseau, and for each sawtooth relative to the numbered gray scales along with the calibrated positions of sawteeth and of the reseaux as well as the observed cyclic repetition of reseau patterns permit the frame to be analytically reassembled very accurately.

Computer-Generated Contour Charts

The selenographic coordinates resulting from the processed film readings are presented herein in the form of contour charts. To facilitate this undertaking, a hybrid version of several digital contouring concepts was developed by using the best feature of each.

Basic to all contouring programs is the technique whereby a grid of equally spaced surface coordinates is generated from randomly spaced surface elevations. Since each coordinate of the grid is equally distant from its neighbors, the grid of surface coordinates can be represented by a matrix of elevations (called the "depth matrix"). Thus, each element of the depth matrix represents an elevation above or below a given reference whereas the location of the element in the matrix corresponds to its location within the grid relative to the grid origin.

The depth matrix generation routine used in this study is best described as utilizing a weighted series of neighboring gradients (each of which is derived from a data point and selected neighboring data points which surround it) to approximate the surface elevation at a grid point. As a result, each element of a depth matrix is representative of all the data used to determine it and is, at best, an approximation which is subject to error. Examinations have shown that the general surface is represented rather accurately by the depth matrix, apparent smoothing appearing in some cases as well as overemphasis in others. Further, the accuracy of the depth matrix is a function of grid point separation and data point density as well as the location of the grid origin relative to the data. The primary advantage of this technique lies in its relative freedom from surface distortions which result from a shift in the positions of surface characteristics when slopes are extrapolated to a grid point.

The technique for contouring utilized in this study is called "grid point scanning." In this technique the rows of the depth matrix are subdivided first into groups of three, each with the last row of each group being repeated as the first row in the following group. In a similar fashion, the columns of each group of rows are subdivided into groups of three columns each. In this fashion, the depth matrix is subdivided into a series of 3×3 submatrices each of which is considered in turn beginning with the uppermost left submatrix. Thus, the term "grid point scan" is used. Each of the nine elements of a submatrix are considered to represent surface elevations at the vertices of eight adjacent triangles. Thus, the surface represented by the submatrix is approximated by triangular segments of eight intersecting planes each of which can be contoured. The chief advantage of grid point scanning is the fact that all possible contours within each submatrix are drawn.

The plotting routine is responsible for most misrepresentations of the surface especially when it is called upon to interpolate between grid points (linear interpolation is used). In addition, because of the computer's tendency to be exact, two sets of data for the same area which have random uncertainties of a few meters will not yield charts with a one to one correspondence. The foregoing is evident when it is recognized that a contour represents a boundary between those elevations with magnitudes greater than an integral multiple of the contour interval and those elevations with smaller magnitudes. They will, however, be similar and portray the same general surface characteristics.

Frequency Distribution Curves

To compare two solutions, a digital program was written whereby both the absolute and relative uncertainties in positions of features could be studied statistically. To compare two sets of data, the computer was instructed to first scan the data to determine those points which were common to both sets and obtain the differences. This first difference represents an uncertainty in absolute coordinates. However, in certain cases, the absolute coordinates will be in error whereas the relative coordinates will be very accurate. As a result, the computer was instructed to calculate a relative uncertainty based on the following expression:

$$\delta\Delta U_{i,i+n} = \left(U_{i,l} - U_{i+n,l}\right) - \left(U_{i,m} - U_{i+n,m}\right) \tag{7}$$

where the difference $\delta\Delta U_{i,i+n}$ represents the relative uncertainty between the coordinates (U represents the particular coordinate, R, Φ, λ, and so forth) resulting from different solutions l and m. The differences are obtained for all combinations of points (as indicated by the subscripts i and $i+n$).

To determine the most probable uncertainty in absolute and relative position, the differences are grouped and plotted as frequency distribution curves. Points on the frequency distribution curve are determined as being the total number of discrepancies determined by equation (7) with magnitudes which lie within the boundaries

$$U_g - \frac{\delta U}{2} \leqq \delta \Delta U_{i,i+n} \leqq U_g + \frac{\delta U}{2} \tag{8}$$

where U_g is the mean discrepancy in the coordinate U and δU is a preassigned variable.

For all solutions compared, frequency distributions of the discrepancies in the absolute and relative magnitudes of radius, latitude, and longitude were plotted. In each case the incremental discrepancy δU (least mean value) in radius was taken to be ±100 meters, whereas that for each of the selenographic coordinates (latitude and longitude) was taken to be $0^{\circ}.002$ (60 meters), respectively. The resulting frequency distribution curves were not normalized and were computer generated.

PRESENTATION OF RESULTS

In this study frequency distribution curves as well as contour charts have been used in an attempt to determine whether there is a serious loss of accuracy when using a block solution. To achieve this objective, the three photographic sequences II P-8A, II P-8B, and II P-8C covering site II P-8 were chosen for the purpose of comparison since sequence II P-8A overlapped sequence II P-8B by approximately 70 percent and sequence II P-8C, by approximately 35 percent. The three orbital passes were consecutive and were computed from a common data arc. The camera attitudes for each sequence were near normal (0°), that of sequence C being greater than sequence B and that of sequence B being greater than sequence A. The total lunar terrain covered by the three sequences was roughly a 50-km square.

Although numerical estimates to various apparent biases, and so forth, are made from time to time during the discussion which follows this section, a quantitative comparison of the accuracy of the block and strip solutions was not the objective of this study. It was desired to determine, qualitatively, the adequacy of a block solution. In view of the advantages of a block solution as opposed to those of several strip solutions (discussed earlier), the failure or success of the block solution to be adequately representative of all its parts (sequences) is one criteria for assessing its merits. Also, those block solutions which result from combining various sequences of photographic data must compare favorably with each other if a block solution is to be the preferred solution.

To accomplish these assessments, both frequency distribution curves and contour charts were obtained for each of the three strips for site II P-8 and for various combinations of the three strips. The frequency distribution curves allowed for a comparison of the actual unfiltered selenographic coordinates (radius, latitude, and longitude) and each is presented and discussed in detail in appendix B. (See figs. 6, 17 to 26.) In figure 5, those frequency distributions considered to be representative of the results in appendix B are presented to facilitate the comparisons of strip and block solutions and are discussed in a separate section. The contour charts for each of the various solutions involving the three sequences for site II P-8 are presented in appendix C (figs. 9, 27 to 36) and are discussed briefly along with figure 5.

A secondary objective of this paper was to estimate the absolute uncertainty in the resulting selenographic coordinates. To accomplish this objective, those solutions involving data from photograph sequences I P-5, II P-8, and II P-7 were compared with that solution for III P-7. The frequency distribution curves and contour charts for each are presented in appendixes B and C, respectively. That frequency distribution curve for the comparison of II P-8 with III P-7A and III P-7B was found to be representative of these comparisons and is shown in figure 6 for the purpose of discussion.

Finally, in figures 7 to 11, the contour charts for the five original Apollo landing sites are shown and in figures 12 to 15 photographs covering the areas represented in figures 7 to 10 are shown. In figure 16, a frequency distribution of the discrepancies existing between the elevation predicted by the contour chart and the true elevation is presented for the purpose of showing the quality of the fit.

DISCUSSION

The frequency distribution curves are useful tools for determining qualitatively how well two different solutions agree. However, the two solutions have systematic biases from a variety of sources which cannot be separated from the data. Furthermore, frequency distribution curves resulting from a comparison of two solutions will not give a normally distributed curve (Gaussian distribution) since the differences between measurements are plotted rather than the distribution of measurements about the mean of a common observable. If it is assumed that the photographic data is flawless for each sequence, the terrain models obtained from each would be essentially identical except for distortions due to uncertainties in camera attitude (which results in the two models being inclined with respect to each other) and for displacements in model location due to orbital biases. In the event of an attitude uncertainty, the frequency distribution curves will be flattened and slightly shifted from the zero line of symmetry with some possible loss of symmetry. A shift in the line of symmetry will, also, be the result of orbital uncertainties and an

uneven distribution of features about the axis of intersection of the two terrain models. Thus, standard deviations in the usual sense will be meaningless here and, as such, will not be employed. However, in reference 11 the standard deviation of a frequency distribution is shown to be approximately one-half the total spread at approximately 0.6 times its peak value. Thus, the standard deviation, as defined here, will be taken as a basis for measuring the "spread" of the curves.

For each comparison, frequency distribution curves for the absolute and relative differences in radius, latitude, and longitude were plotted (a total of six curves). For each, the line of symmetry (the coordinate on the abscissa at which the curve reaches a peak), curve shape (the rapidity with which the peak is reached and the spread of differences) and curve broadness (spread) are characteristics considered to be most important. The curve shape is, perhaps, the more misleading of the characteristics, as will be seen during the course of the discussion which is to follow. It is, however, important to remember that the coordinates of each point on the curve represents that number of times that selenographic coordinates of features which are common to two solutions were found to have differences within the boundaries defined by a value on the abscissa and its least mean value (or least difference).

Comparison of Strip and Block Solutions

Those frequency distribution curves resulting from a comparison of the strip and block solutions listed in table I are presented and are discussed in appendix B. The contour charts for each are discussed in appendix C and are not compared here.

TABLE I.- NUMBER OF COMMON FEATURES IN VARIOUS STRIP AND BLOCK SOLUTIONS USED FOR COMPARISON

Mission			III	II								I
I	Strip								P-8C	P-8B	P-8A	P-5
		Block	P-7AB	P-7AB	P-8ABC	P-8BC	P-8AC	P-8AB				
	P-5		70	0	155	155	141	116	140	104	58	268
II	P-8A		136	0	173	128	170	172	53	124	175	
	P-8B		110	0	190	191	182	189	109	191		
	P-8C		45	0	145	146	145	112	147			
		P-8AB	147	0	220	195	233	243				
		P-8AC	146	0	264	219	266					
		P-8BC	115	0	233	237						
		P-8ABC	152	0	282							
		P-7AB	21	252								
III		P-7AB	242									

In appendix B, it is shown that the two strips for sites II P-8A and II P-8B compare reasonably well with each other and that the comparison of site II P-8C with each of sites II P-8A and II P-8B is least favorable. Thus, figures 19, 20, 22, and 23 are selected as being representative of the remaining figures and are shown together in figure 5 for the purpose of comparison. Each comparison in figure 5 involves sequence II P-8C either as a strip solution or as a part of a block solution.

In appendix B, it was found that the absolute and relative radial uncertainties (approximately ±300 meters) are very small, while the lines of symmetry are very near zero. For figure 5(c) and in figure 19, where the comparisons of site II P-8B with site II P-8C are shown, it was determined that the absolute radial uncertainty is biased about the 600-meter ordinate. Further, the spread of uncertainties for each of the comparisons of strip solutions remained essentially the same for the absolute distributions and, for the relative distributions, the spread was observed to diminish somewhat. The disagreements are probably the results of the combined effect of orbital uncertainties and of an incomplete solution to camera attitude. Further, the spread in the radial uncertainty was sufficiently large to permit a one-to-one correspondence between contour charts to be an unreasonable expectation. Thus, the strip solutions are seen to be inconsistent.

Since strip C did not compare favorably with either strip A or strip B, those block solutions requiring its use were studied. Further, they were compared with strip B since strip B is common to both strips C and A; as a result, the number of common features remains fixed from comparison to comparison. Thus, it is possible to determine whether the block solution has improved the results.

In figures 5(a) and 20, the block solution for site II P-8BC is compared with the strip solution for site II P-8B. As can be seen from the curves involving the absolute coordinates, the comparison is an excellent one, since the frequency distribution curves have extremely sharp peaks for latitude, radius, and longitude. The radial spread was found to be approximately ±100 meters as opposed to ±300 for strips A and B and ±600 for strips B and C, a significant improvement.

In figure 5(d), the block solution II P-8BC is compared with that of II P-8AC and the agreement is found to be excellent. Further, in figure 5(b), a block solution involving all three sequences in site II P-8 is compared with that block solution II P-8BC with excellent results. In fact, no comparison with the strip solutions gave poor results. Also, spreads were practically nonexistent.

In general, it is seen that the uncertainties in selenographic radius, as determined by comparing various block solutions with various strip solutions and other block solutions, are of the order of 200 meters, and the uncertainties in latitude and longitude rarely exceed $0^{\circ}.01$ (300 meters). In addition, when the individual curves in figures 20 to 24 were compared with each other, a striking similarity was noted. Thus, it is concluded

that block solutions determined from sequences of photographs which have been exposed from consecutive orbital passes determined from the same orbital parameters, consistently give better results than those obtained from strip solutions. Consequently, in view of the striking similarities existing between the various figures, the more complete solution to camera attitude, and the larger available sample of data, block solutions are to be preferred over strip solutions.

Comparison of Block Solutions From Different Missions and Data Arcs

As has been pointed out, a small section of Sinus Medii was photographed from missions I, II, and III and are denoted by the site identification I P-5, II P-8, and III P-7, respectively. In addition, sites II P-7A and II P-7B were above and adjacent to site II P-8. Because of the higher orbital inclination of mission III, segments of both sites II P-7 and II P-8 were contained in site III P-7. Thus, site III P-7 was used as a reference to compare the discrepancies in selenographic coordinates resulting from orbital data determined from different missions and different data arcs. It should, however, be pointed out that the results were for particular cases and can in no way be interpreted as being representative of all discrepancies expected between different missions and data arcs. They were, however, utilized to gain an insight into the biases existing between results of different missions, and so forth and to estimate the uncertainty in absolute position of lunar features. (Absolute in this sense means the true position of the feature.) As before, frequency distribution curves were utilized and are discussed in appendix B.

The results of site II P-8 are typical and are shown in figure 6 for the purpose of discussion. The relative uncertainties for each coordinate were found to be nearly symmetrical about zero although the absolute uncertainties, in some cases, exhibited rather large biases (a displacement of the line of symmetry). The relative radial uncertainty was nearly symmetrical about zero for each case with the spread in figure 6 of ±600 meters (a worst case) differing from comparison to comparison. A bias of $0^{\circ}.06$ (1.8 km) was noted for the mission I comparison of absolute latitude whereas the remaining latitude biases remained essentially the same ($0^{\circ}.01$ or 0.3 km). The bias in absolute longitude remained at $0^{\circ}.03$ (0.9 km) for each comparison.

Also, biases in both absolute and relative distributions were of the same sign for all comparisons. Thus, with the exception of the absolute latitude bias in I P-5, the data appear to be in good agreement with that of site II P-7 and yield essentially the same results as is shown in figure 6. (See appendix B.) It is regrettable that so few common points were identified between sites II P-7 and III P-7 since more points would probably have shown even better agreement between the three comparisons.

An uncertainty in radius can be the result of many errors, especially when the identified features are concentrated near the edges of the photographs as in site II P-7.

Since site III P-7 was rolled out of the orbital plane approximately 28^{o}, the effects of optical distortions, read out system distortions, and so forth will be more effective. Thus, the spread in the radial component could be affected by these distortions as well as slight residuals in the attitude.

Thus, in view of the foregoing conditions, it is concluded that two different (both adjacent) data arcs from the same mission can yield results which are in good agreement. Also, results from different missions can be biased significantly in either latitude, longitude, or (to be general) both. These uncertainties can be effectively eliminated by applying corrections to the appropriate biased coordinates for all the features in each solution. Such a correction would however be difficult to determine in an absolute sense and must be applied in such a way as to avoid distorting the respective models. A visual examination of other results has shown that the uncertainties existing between results of different missions is consistent with those discussed here. Thus, such a correction would necessarily be determined by feature matching.

As for the absolute uncertainties in the selenographic coordinates, it is necessary to turn to reference 11. In reference 11 it was shown that the standard deviation of the difference in the means of two estimates to a variable is equal to the root sum square of the standard deviations of the mean of each. Since each frequency distribution represents a distribution of the differences between two estimates to a selenographic coordinate which are assumed to be equally probable (the spread is assumed to be a result of orbital errors), the standard deviation of each are assumed to be equal and the standard deviation of each coordinate is estimated to be approximately the square root of one-half the square of the spread in each distribution. Since the larger spread in distribution is assumed to represent the maximum expected uncertainty for a coordinate, for latitude the maximum 1σ uncertainty is estimated to be $0^{o}.01$ (300 meters); for longitude the maximum 1σ uncertainty is estimated to be $0^{o}.03$ (900 meters); and for the radius a maximum 1σ uncertainty of 430 meters is expected. These results correspond to an estimated absolute uncertainty in position of ± 1 km and appear to be in good agreement with other results published in references 2, 3, and 4.

The Primary Apollo Landing Sites

The foregoing discussion has concerned itself with the various uncertainties existing between those solutions involving film readings from differing missions, consecutive orbits, differing data arcs, and the optimum conditions under which the various solutions might be combined into one integrated solution to the whole. It has been shown that strip solutions, although accurate within themselves, exhibit uncertainties with respect to other strip solutions of the same area. It has also been determined that block solutions involving film readings from photographs exposed from consecutive orbits are an accurate

representation of the various strip solutions and are to be preferred over strip solutions. Thus, since the primary pre-Apollo landing sites were photographed from consecutive orbits or consecutive missions and sometimes both, those strip solutions and, where applicable, block solutions involving photographs from consecutive orbits computed from a common data arc are contoured for the remaining sites.

In figures 7 to 11, the contour charts for the Apollo landing sites 1 to 5, respectively, are shown, and in figures 12 to 15, the mission V photographs for sites 1 to 4 are shown. These sites have the Lunar Orbiter designations of site II P-2, II P-6AB, III P-11, II P-8, and II P-13AB. As can be seen from the figures, the sites are relatively smooth with some minor surface undulations. In no case are these undulations of a radical nature; in fact, the general slope over the whole site never exceeds approximately 1^{o}, and for all practical purposes all sites can be defined as being essentially flat.

The depth matrix from which each chart was determined was checked for accuracy by comparing the elevation predicted by it at each of the data points (features) calculated from film readings. In figure 16, the frequency distribution of the resulting differences are shown for one chart. Since 67 percent of the points fell within a spread of ±100 meters, the matrix is a very good representation of the data. Similar plots were obtained for 16 other charts.

The contour chart in figure 8 and the results required to obtain it were utilized extensively along with charts produced by other agencies (Aeronautical Chart and Information Center, The Army Map Service, and so forth) to evaluate the general surface characteristics (direction of slope, magnitude of slope and so forth) of the first Apollo landing site (site 2). The contours were also used to obtain approach profiles along the direction of the landing path in partial support of the first manned lunar landing.

CONCLUDING REMARKS

Throughout the foregoing discussion, the uncertainties in selenographic radius, latitude, and longitude resulting from film readings obtained from photographs exposed from consecutive orbits of the same mission, different data arcs, and different missions have been compared by using frequency distribution curves and contour charts. Also, those block solutions resulting from film readings involving all the photographs from all consecutive orbits determined on the same data arc were compared with strip solutions involving the same data as well as strip and block solutions resulting from different missions and data arcs. Thus, those conditions under which results from different missions and data arcs may be combined into one set of consistent results were investigated.

The results of this study has shown that significant differences, although not large, do exist between various strip solutions involving data from consecutive orbits determined

from a common data arc. Furthermore, a block solution, involving the same data, will minimize these discrepancies as well as produce internally consistent results covering a larger area. Thus, it is concluded that the block solution is to be preferred over the strip solution.

Block solutions from different missions were found to exhibit significant and, sometimes, large biases in at least one of the selenographic coordinates; such biases imply orbital errors. As a result, it is concluded that these discrepancies can be eliminated by applying an appropriate correction to the particular coordinate of each of the features in each solution.

The block and strip solutions for the primary Apollo landing sites photographed from mission II were processed and contoured. The resulting contour charts show the sites to be relatively smooth (flat).

Langley Research Center,
National Aeronautics and Space Administration,
Hampton, Va., May 4, 1970.

APPENDIX A

PARTIAL DERIVATIVES OF "Q" CONDITION

In the text Q is defined as

$$Q\left(\bar{\rho}_{i,j},\bar{\rho}_{i,k},\bar{R}_j,\bar{R}_k\right) = \left(\bar{\rho}_{i,j} \times \bar{\rho}_{i,k}\right) \cdot \bar{\Delta} = \left(\bar{\rho}_{i,j} \times \bar{\rho}_{i,k}\right) \cdot \left(\left(\bar{R}_j + \bar{\rho}_{i,j}\right) - \left(\bar{R}_k + \bar{\rho}_{i,k}\right)\right)$$

by equation (2). Upon linearization,

$$Q = \underline{Q} + Q'$$

where $\underline{Q}$ is an approximate value of Q and Q' is the function of partial derivatives of Q with respect to each of the camera attitude components and the spacecraft height H_o.

In this appendix, each of the partial derivatives of Q in terms of $\rho_{i,j}$, $\rho_{i,k}$, and so forth are given without explanation. The partials of $\rho_{i,j}$ and so forth are given in the appendix of reference 1 and are not repeated.

The partial derivatives of Q are as follows:

$$\frac{\partial Q_{i,j_u,k_v}}{\partial \theta_u} = \left[\left(R_{x,j_u} + \rho_{x,i,j_u}\right) - \left(R_{x,k_v} + \rho_{x,i,k_v}\right)\right]\left(\rho_{z,i,k_v}\frac{\partial \rho_{y,i,j_u}}{\partial \theta_u} - \rho_{z,i,j_u}\frac{\partial \rho_{y,i,k_v}}{\partial \theta_u}\right)$$

$$+ \left[\left(R_{y,j_u} + \rho_{y,i,j_u}\right) - \left(R_{y,k_v} + \rho_{y,i,k_v}\right)\right]\left(\rho_{z,i,j_u}\frac{\partial \rho_{x,i,k_v}}{\partial \theta_u} - \rho_{z,i,k_v}\frac{\partial \rho_{x,i,j_u}}{\partial \theta_u}\right)$$

$$+ \left[\left(R_{z,j_u} + \rho_{z,i,j_u}\right) - \left(R_{z,k_v} + \rho_{z,i,k_v}\right)\right]\left[\left(\rho_{x,i,j_u}\frac{\partial \rho_{y,i,k_v}}{\partial \theta_u} - \rho_{x,i,k_v}\frac{\partial \rho_{y,i,j_u}}{\partial \theta_u}\right)\right.$$

$$\left. + \left(\rho_{y,i,k_v}\frac{\partial \rho_{x,i,j_u}}{\partial \theta_u} - \rho_{y,i,j_u}\frac{\partial \rho_{x,i,k_v}}{\partial \theta_u}\right)\right]$$

$$\frac{\partial Q_{i,j_u,k_v}}{\partial \tau_u} = \left[\left(R_{x,j_u} + \rho_{x,i,j_u}\right) - \left(R_{x,k_v} + \rho_{x,i,k_v}\right)\right]\left(\rho_{z,i,k_v}\frac{\partial \rho_{y,i,j_u}}{\partial \tau_u} - \rho_{z,i,j_u}\frac{\partial \rho_{y,i,k_v}}{\partial \tau_u}\right)$$

$$+ \left[\left(R_{y,j_u} + \rho_{y,i,j_u}\right) - \left(R_{y,k_v} + \rho_{y,i,k_v}\right)\right]\left(\rho_{z,i,j_u}\frac{\partial \rho_{x,i,k_v}}{\partial \tau_u} - \rho_{z,i,k_v}\frac{\partial \rho_{x,i,j_u}}{\partial \tau_u}\right)$$

$$+ \left[\left(R_{z,j_u} + \rho_{z,i,j_u}\right) - \left(R_{z,k_v} + \rho_{z,i,k_v}\right)\right]\left[\left(\rho_{x,i,j_u}\frac{\partial \rho_{y,i,k_v}}{\partial \tau_u} - \rho_{x,i,k_v}\frac{\partial \rho_{y,i,j_u}}{\partial \tau_u}\right)\right.$$

$$\left. + \left(\rho_{y,i,k_v}\frac{\partial \rho_{x,i,j_u}}{\partial \tau_u} - \rho_{y,i,j_u}\frac{\partial \rho_{x,i,k_v}}{\partial \tau_u}\right)\right]$$

$$\frac{\partial Q_{i,j_u,k_v}}{\partial \varphi_u} = \left[\left(R_{x,j_u} + \rho_{x,i,j_u}\right) - \left(R_{x,k_v} + \rho_{x,i,k_v}\right)\right]\left(\rho_{z,i,k_v}\frac{\partial \rho_{y,i,j_u}}{\partial \varphi_u} - \rho_{z,i,j_u}\frac{\partial \rho_{y,i,k_v}}{\partial \varphi_u}\right)$$

$$+ \left[\left(R_{y,j_u} + \rho_{y,i,j_u}\right) - \left(R_{y,k_v} + \rho_{y,i,k_v}\right)\right]\left(\rho_{z,i,j_u}\frac{\partial \rho_{x,i,k_v}}{\partial \varphi_u} - \rho_{z,i,k_v}\frac{\partial \rho_{x,i,j_u}}{\partial \varphi_u}\right)$$

$$+ \left[\left(R_{z,j_u} + \rho_{z,i,j_u}\right) - \left(R_{z,k_v} + \rho_{z,i,k_v}\right)\right]\left[\left(\rho_{x,i,j_u}\frac{\partial \rho_{y,i,k_v}}{\partial \varphi_u} - \rho_{x,i,k_v}\frac{\partial \rho_{y,i,j_u}}{\partial \varphi_u}\right)\right.$$

$$\left. + \left(\rho_{y,i,k_v}\frac{\partial \rho_{x,i,j_u}}{\partial \varphi_u} - \rho_{y,i,j_u}\frac{\partial \rho_{x,i,k_v}}{\partial \varphi_u}\right)\right]$$

$$\frac{\partial Q_{i,j_u,k_v}}{\partial H_{o,i}} = \left[\left(R_{x,j_u} + \rho_{x,i,j_u}\right) - \left(R_{x,k_v} + \rho_{x,i,k_v}\right)\right]\left(\rho_{z,i,k_v}\frac{\partial \rho_{y,i,j_u}}{\partial H_{o,i}} - \rho_{z,i,j_u}\frac{\partial \rho_{y,i,k_v}}{\partial H_{o,i}}\right)$$

$$+ \left[\left(R_{y,j_u} + \rho_{y,i,j_u}\right) - \left(R_{y,k_v} + \rho_{y,i,k_v}\right)\right]\left(\rho_{z,i,j_u}\frac{\partial \rho_{x,i,k_v}}{\partial H_{o,i}} - \rho_{z,i,k_v}\frac{\partial \rho_{x,i,j_u}}{\partial H_{o,i}}\right)$$

$$+ \left[\left(R_{z,j_u} + \rho_{z,i,j_u}\right) - \left(R_{z,k_v} + \rho_{z,i,k_v}\right)\right]\left[\left(\rho_{x,i,j_u}\frac{\partial \rho_{y,i,k_v}}{\partial H_{o,i}} - \rho_{x,i,k_v}\frac{\partial \rho_{y,i,j_u}}{\partial H_{o,i}}\right)\right.$$

$$\left. + \left(\rho_{y,i,k_v}\frac{\partial \rho_{x,i,j_u}}{\partial H_{o,i}} - \rho_{y,i,j_u}\frac{\partial \rho_{x,i,k_v}}{\partial H_{o,i}}\right)\right]$$

$$- \left[\left(R_{x,j_u} + \rho_{x,i,j_u}\right) - \left(R_{x,k_v} + \rho_{x,i,k_v}\right)\right]\left(\rho_{y,i,j_u} - \rho_{y,i,k_v}\right)$$

$$- \left[\left(R_{y,j_u} + \rho_{y,i,j_u}\right) - \left(R_{y,k_v} + \rho_{y,i,k_v}\right)\right]\left(\rho_{x,i,k_v} - \rho_{x,i,j_u}\right)$$

The partial derivatives of Q with respect to θ_v, τ_v, and φ_v are identical to those for θ_u, τ_u, and φ_u with the exception of the subscript u for each independent variable. Thus, these partial derivatives will not be repeated here.

For each expression it should be remembered that

$$\rho_{z,i,j_u} = -\left(H_{o,i} + R_{z,j_u} - R_{z,o}\right)$$

and

$$\rho_{z,i,k_v} = -\left(H_{o,i} + R_{z,k_v} - R_{z,o}\right)$$

The subscripts were affixed to Q to imply that it is a function of variables which change with point identification, frame number, and sequence number.

APPENDIX B

FREQUENCY DISTRIBUTION CURVES

The frequency distribution curves are a useful tool for determining qualitatively how well two different solutions agree. It should be noted that the two solutions have systematic biases from a variety of sources which cannot be separated from the data. Also, frequency distribution curves resulting from a comparison of two solutions will not give a normally distributed curve (Gaussian distribution) since the differences between measurements are plotted rather than the distribution of measurements about the mean of a common observable. If it is assumed that the photographic data is flawless for each sequence, the terrain models obtained from each would be essentially identical except for distortions due to uncertainties in camera attitude (which results in the two models being inclined with respect to each other) and for displacements in model location due to orbital biases. In the event of an attitude uncertainty, the frequency distribution curves will be flattened and slightly shifted from the zero line of symmetry with some possible loss of symmetry. A shift in the line of symmetry will also be the result of orbital uncertainties and an uneven distribution of features about the axis of intersection of the two terrain models. Thus, standard deviations in the usual sense will be meaningless here and, as such, will not be employed. However, in reference 11 the standard deviation of a frequency distribution is shown to be approximately the coordinate difference defined by the line of symmetry and that ordinate intersecting the curve at 0.6 times its peak value. Thus, the standard deviation, as defined here, will be taken as a basis for measuring the "spread" of the curves.

For each comparison, frequency distribution curves for the absolute and relative differences in radius, latitude, and longitude were plotted (a total of six curves). For each curve, the line of symmetry (the coordinate on the abscissa at which the curve reaches a peak), curve shape (the rapidity with which the peak is reached and the spread of differences), and curve broadness (spread) are characteristics considered to be most important. The curve shape is, perhaps, the more misleading of the characteristics, as will be seen during the course of the discussion which is to follow. It is, however, important to remember that the coordinates of each point on the curve represent that number of times that a selenographic coordinate of features which are common to two solutions was found to have a value within the boundaries defined by a value on the abscissa and its least mean value (or least difference).

Strip Solutions from a Common Data Arc

In figures 17, 18, and 19, those frequency distribution curves resulting from the comparisons of the three strip solutions for sites II P-8A, II P-8B, and II P-8C are plotted.

As can be seen, most of the points fall within a narrow band (peak rapidly). The net uncertainty in both absolute and relative latitude and longitude never exceeds $\pm 0^{\circ}.02$ (roughly 600 meters) with the spread (region of largest concentration) being less and the net uncertainty in radius has a larger variance (spread). In figure 17, the strip solution for site II P-8A is compared with the strip solution for site II P-8B. In this case the spreads in the absolute and relative radial uncertainties (approximately ±300 meters) are very small whereas the lines of symmetry are very near zero. Thus, II P-8A and II P-8B are considered to be in good agreement. In figures 18 and 19 the strip solutions for site II P-8C is compared with strip solutions for site II P-8A and II P-8B. As can be seen, the curves in each differ only slightly. In figure 18 it is seen that the absolute radial uncertainty is symmetrical about the 800-meter ordinate (biased) whereas in figure 19 the absolute radial uncertainty is biased about the 600-meter ordinate. In each figure, the spread of uncertainties compare well for each curve and there is some improvement in the relative uncertainties. The results in figure 18 obtained by using the strip for site II P-8C suffer from too few common features (a total of 52) and from an insufficient sidelap (approximately 30 percent) as well as other factors. However, from figure 19 and these observations, it must be stated that II P-8C does not agree well with II P-8A and II P-8B. The disagreement is probably a combination of a buildup in relative cross-orbital uncertainties and of an incomplete attitude solution. Thus, it is seen that strip solutions do not necessarily yield the more consistent results. In each figure, the relative radius has sufficient spread to permit a one-to-one correspondence between contour charts to be an unreasonable expectation. However, it is to be expected that the general characteristics of the surface will be preserved, that is to say, flat areas and general direction of slope should be seen in the same locations in different charts. (See appendix C.)

The foregoing discussion has concerned itself with the uncertainties between strip solutions obtained from sequences of photography taken from consecutive orbital passes determined from the same data arc. In summary, it can be stated that the results have shown the selenographic radius at the feature to be uncertain by approximately 300 meters for adjacent strips, and the selenographic latitude and longitude to have uncertainties of approximately 450 meters or $0^{\circ}.015$. The larger absolute radial uncertainty (800 meters) between strips II P-8A and II P-8C can be partly attributed to increasing relative orbital uncertainties resulting from the two-orbit separation.

Block Solutions

It is now desirable to look at the various block solutions resulting from combinations of strips A, B, and C. Since strip C did not compare favorably with either strip A or B, those block solutions resulting from its use are studied. Also, they will be compared with strip B since strip B is common to both strips C and A which will result in the

number of common features remaining fixed from comparison to comparison. Thus, it will be possible to determine whether the block solution has improved the results.

In figure 20, the block solution II P-8BC is compared with the strip solution II P-8B. As can be seen from the curves involving the absolute coordinates, the comparison is an excellent one, since the frequency distribution curves have extremely sharp peaks for latitude, radius, and longitude. The radial spread is approximately ±100 meters as opposed to ±300 meters for A and B and ±600 meters for B and C, a significant improvement. In figure 21, the block solution involving the sequences A and C was compared with the strip solution II P-8B. Once again the comparisons are excellent, except that there is a slightly wider spread in the frequency distribution of selenographic radii. However, since the block solution II P-8AC (fig. 21) involved sequences of photography which contained only 52 common points (see table I) whereas that of II P-8BC (fig. 20) contained 128 points, the block solution II P-8BC is considered to be a better solution than that for II P-8AC. Thus, the comparison of II P-8AC with II P-8B is expected to imply larger discrepancies. Thus, it is concluded that the block solutions which utilize data obtained from the same mission and a common data arc will improve the results.

In figure 22, the block solution II P-8BC is compared with that of II P-8AC and the agreement is found to be excellent. Also, in figure 23, a block solution involving all three sequences in site II P-8 is compared with that block solution II P-8BC and in figure 24 it is compared with that strip solution involving sequence II P-8A with excellent results in each case. In fact, no comparison with the remaining strip solutions gave poor results. Furthermore, spreads were practically nonexistent.

In general, it is seen that the uncertainties in selenographic radius, as determined by comparing various block solutions with various strip solutions and other block solutions, uncertainties in selenographic radius are of the order of 200 meters, and the uncertainties in latitude and longitude rarely exceed $0^{\circ}.001$ (300 meters). In addition, when the individual curves in figures 20 to 24 are compared with each other, a striking similarity is noted. Thus, from the foregoing, it is concluded that block solutions determined from sequences of photographs which have been exposed from consecutive orbits determined from the same orbital parameters, consistently give results which are more accurate than those obtained from strip solutions. Consequently, in view of the striking similarities existing between the various figures, the more complete solution to camera attitude, and the larger available sample of data, block solutions are to be preferred over strip solutions.

Comparison of Block Solutions from Different Missions and Data Arcs

As has been pointed out, a small section of Sinus Medii was photographed from missions I, II, and III and are denoted by the site identification I P-5, II P-8, and III P-7,

respectively. In addition, sites II P-7A and II P-7B were photographed and were above and adjacent to site II P-8. Because of the higher orbital inclination of mission III, segments of both sites, II P-7 and II P-8, were contained in III P-7. Thus, if site III P-7 should be used as a reference, the discrepancies in selenographic coordinates resulting from orbital data determined from different missions and different data arcs can be compared. However, these results are for particular cases and can in no way be interpreted as being wholly representative of the discrepancies to be expected between the different missions and data arcs in a general sense. They will, however, be utilized to study the biases existing between results of different missions, and so forth, and to determine an estimate of the uncertainty in absolute position of lunar features. (Absolute in this sense means the true position of the feature.) As before, frequency distribution curves are utilized and are shown in figures 6, 25, and 26.

In figures 6 and 25, results from missions I and II are compared with those from mission III. In each case, the relative uncertainties for each coordinate are seen to be nearly symmetrical about zero, whereas the absolute uncertainties, in some cases, exhibit rather large biases (a displacement of the line of symmetry). In each figure the relative radial uncertainty is nearly symmetrical about zero. The comparison of mission II with mission III (fig. 6) indicates a spread of ±600 meters (a worst case). In the case of latitude and longitude biases, however, the largest bias is in the absolute latitude $0^{\circ}.06$ or 1800 meters (fig. 25) for mission I, whereas each (figs. 6, 25, and 26) seem to exhibit essentially the same in absolute longitude ($0^{\circ}.03$ or 900 meters). The bias in the absolute latitude for both figures 6 and 26 is approximately $0^{\circ}.01$ (300 meters).

It is of interest to note that the spread in the relative radial uncertainty is approximately of the same magnitude in both figures 6 and 25. Furthermore, biases in both absolute and relative distributions are of the same sign for all figures. Also, the bias and spread in the longitude curves for each figure differ only slightly. Thus, with the exception of the absolute latitude bias in I P-5 and the spread in the distributions for figures 6 and 25, the mission II and mission I data appear to be in good agreement with each other.

In the case of figure 26, in which site II P-7 is compared with site III P-7, both the latitude and longitude uncertainties are seen to be shifted in the same direction and to have approximately the same lines of symmetry as those of figure 6 in which site II P-8 is compared with site II P-7. The only real difference is in the spread of the radial curve. It is regrettable that so few common points were identified between sites II P-7 and III P-7 since more points would probably have shown even better agreement between the three figures.

An uncertainty in radius can be the result of many errors, especially when the identified features are concentrated near the edges of the photographs as in those for site II P-7. Since site III P-7 was rolled out of the orbital plane approximately 28°, the

effects of optical distortions, read out system distortions, and so forth will be more effective. Thus, the spread in the radial component could be affected by these distortions as well as by slight residuals in the attitude.

In view of the foregoing, it is concluded that two different (both adjacent) data arcs from the same mission yield results which are in good agreement. Further, results from different missions can be biased significantly in either latitude, longitude, or (to be general) both. The latter uncertainties can be effectively eliminated by applying corrections to the appropriate biased coordinates for all the features in each solution. Such a correction would however be difficult to determine in an absolute sense and must be applied in such a way as to avoid distorting the respective models. A visual examination of other results has shown that the uncertainties existing between results of different missions are consistent with those discussed here. Thus, such a correction would necessarily be determined by feature matching.

APPENDIX C

CONTOUR CHARTS

In figures 27, 28, and 29, contour charts for each of the strip solutions for II P-8A, II P-8B, and II P-8C are shown, and in figure 30 a contour chart resulting from the weighted mean of the selenographic coordinates from each of the three strip solutions is shown. In figures 27 and 28, the regions are seen to be (in both figures) relatively flat. In figure 10, the strip solution II P-8C seems to continue the same trends.

In figure 30, the general characteristics of each of the three strip solutions can be seen. However, this contour chart illustrates a very important point which has been made in the text regarding one-to-one correspondence between contour charts. In figure 29, a series of contour lines run nearly vertically down the center of the chart. In figure 30, the lines are seen to run in a slightly different direction. Even so, if one should compare the elevation at a particular point in figure 30 with its counterpart in figure 29 the results will be very favorable.

In figure 9, the block solution II P-8ABC is contoured. If it should be compared with those contours in figures 27, 28, and 29, similarities will be noted. However, an exact one-to-one correspondence of contour line should not be expected. Where there are depressions on one chart, there are depressions on the other, especially if the depressions are significant. Such a depression clearly defined on one chart may on the other appear between two knolls, which is the case with that depression in figure 29 which occurs at -1° longitude and $-0^{\circ}.5$ latitude. In figures 31, 32, and 33, the contour charts on the block solutions II P-8AB, II P-8BC, and II P-8AC, respectively, are shown for interest and are not discussed further.

In figures 34, 35, and 36, the contour charts for I P-5, III P-7, and II P-7 are shown. A comparison of the charts will reveal similarities, especially between I P-5 and those charts resulting from the sequences in II P-8 (a fact indicated by the similarity of the relative distribution of radial uncertainties discussed in appendix B). In figures 35 and 36, it will be noted that there is very little area common to both charts.

REFERENCES

1. Jones, Ruben L.: An Analytical Study of Lunar Surface Shape and Size From Lunar Orbiter Mission I Photographs. NASA TN D-5243, 1969.

2. Hansen, T. J.: Lunar Orbiter Photo Site Accuracy Analysis – Photo Site Analysis. NASA CR-66734-1, 1968.

3. Hansen, T. J.: Lunar Orbiter Photo Site Accuracy Analysis – Supporting Data. NASA CR-66734-2, 1968.

4. Dyer, John P.: Lunar Orbiter Photo Site Accuracy Analysis – Error Analysis. NASA CR-66734-3, 1968.

5. Boeing Co.: Lunar Orbiter II – Photographic Mission Summary. NASA CR-883, 1967.

6. Moyers, W. G.: Lunar Orbiter Improved Photo Support Data – Lunar Orbiter I. NASA CR-66735-1, 1969.

7. Moyers, W. G.: Lunar Orbiter Improved Photo Support Data – Lunar Orbiter II. NASA CR-66735-2, 1969.

8. Moyers, W. G.: Lunar Orbiter Improved Photo Support Data – Lunar Orbiter III. NASA CR-66735-3, 1969.

9. Moyers, W. G.: Lunar Orbiter Improved Photo Support Data – Lunar Orbiter IV. NASA CR-66735-4, 1969.

10. Moyers, W. G.: Lunar Orbiter Improved Photo Support Data – Lunar Orbiter V. NASA CR-66735-5, 1969.

11. Worthing, Archie G.; and Geffner, Joseph: Treatment of Experimental Data. John Wiley & Sons, Inc., c.1943.

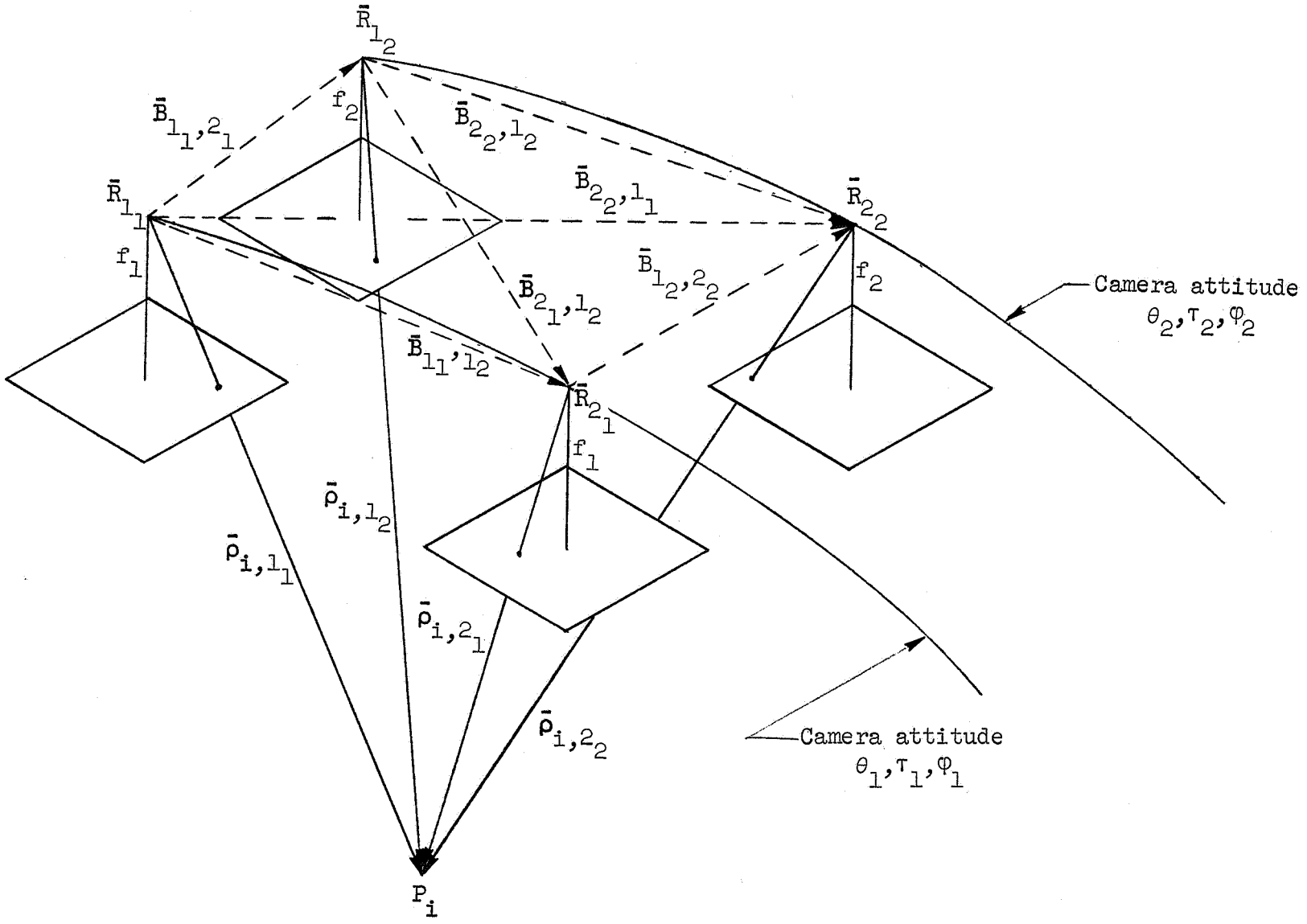

Figure 1.- Vectorial relations between photographs exposed from different orbits.

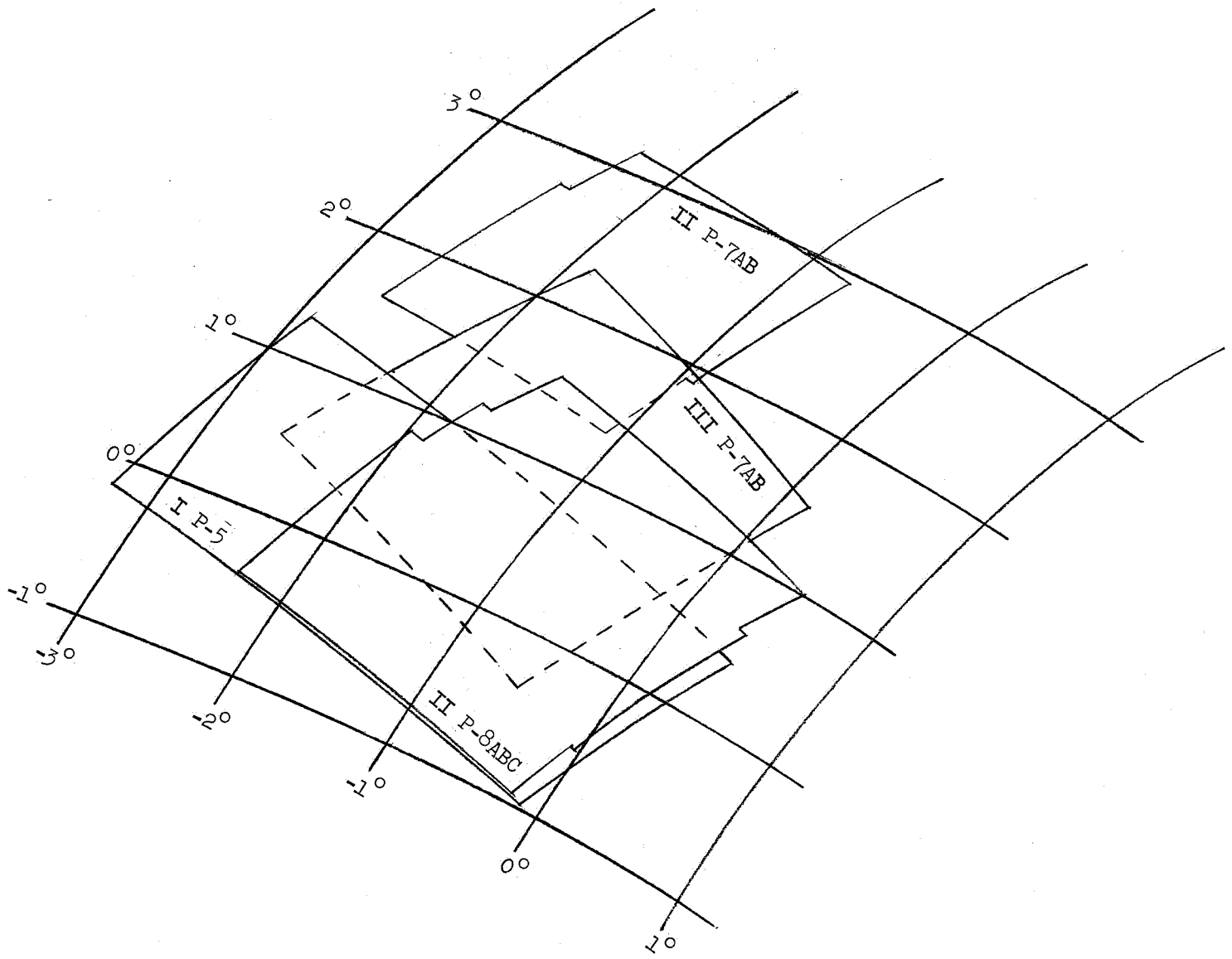

Figure 2.- Approximate location of each photographic strip exposed in the vicinity of Sinus Medii.

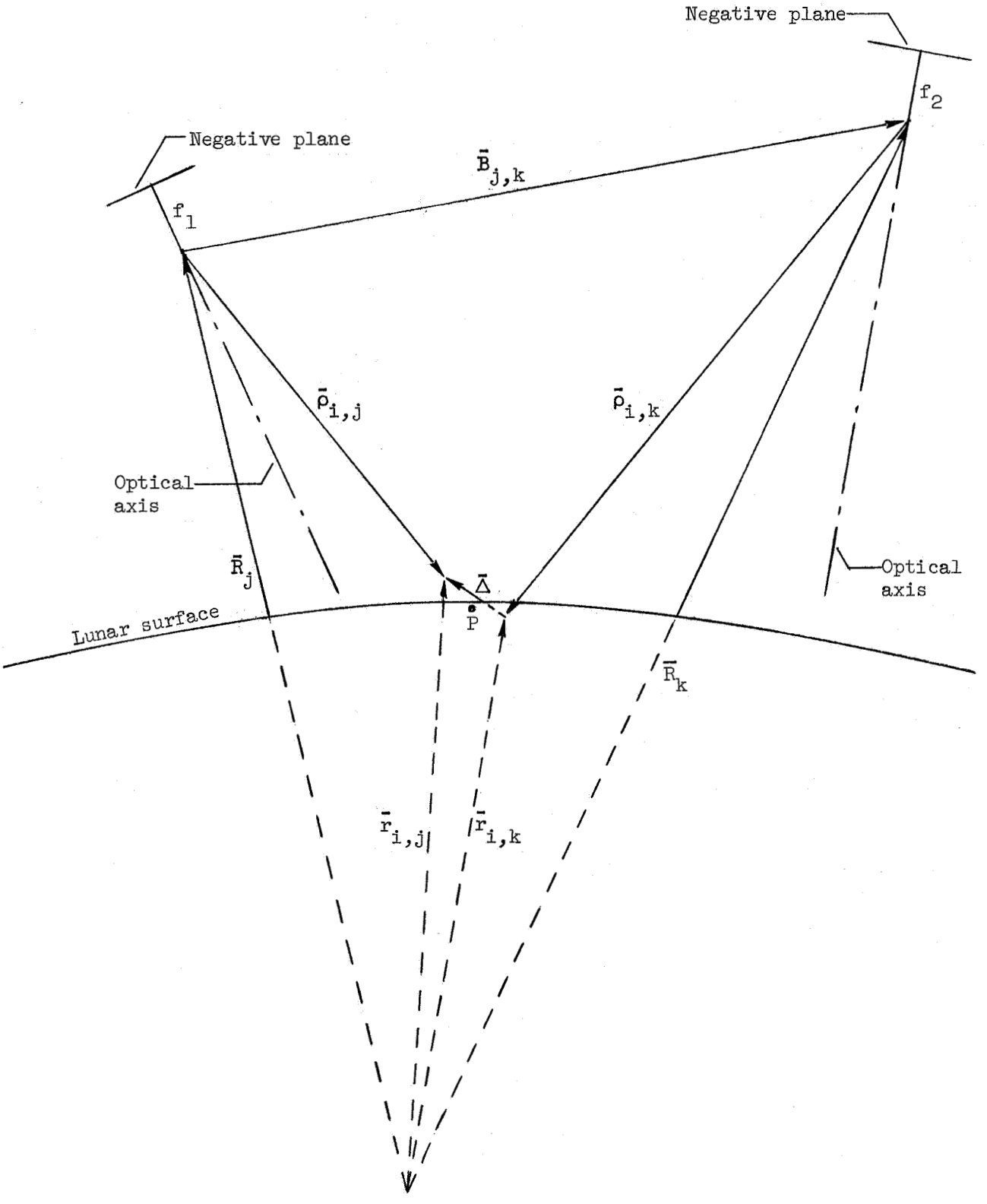

Figure 3.- Pictorial representation of vectorial relations existing between two photographs.

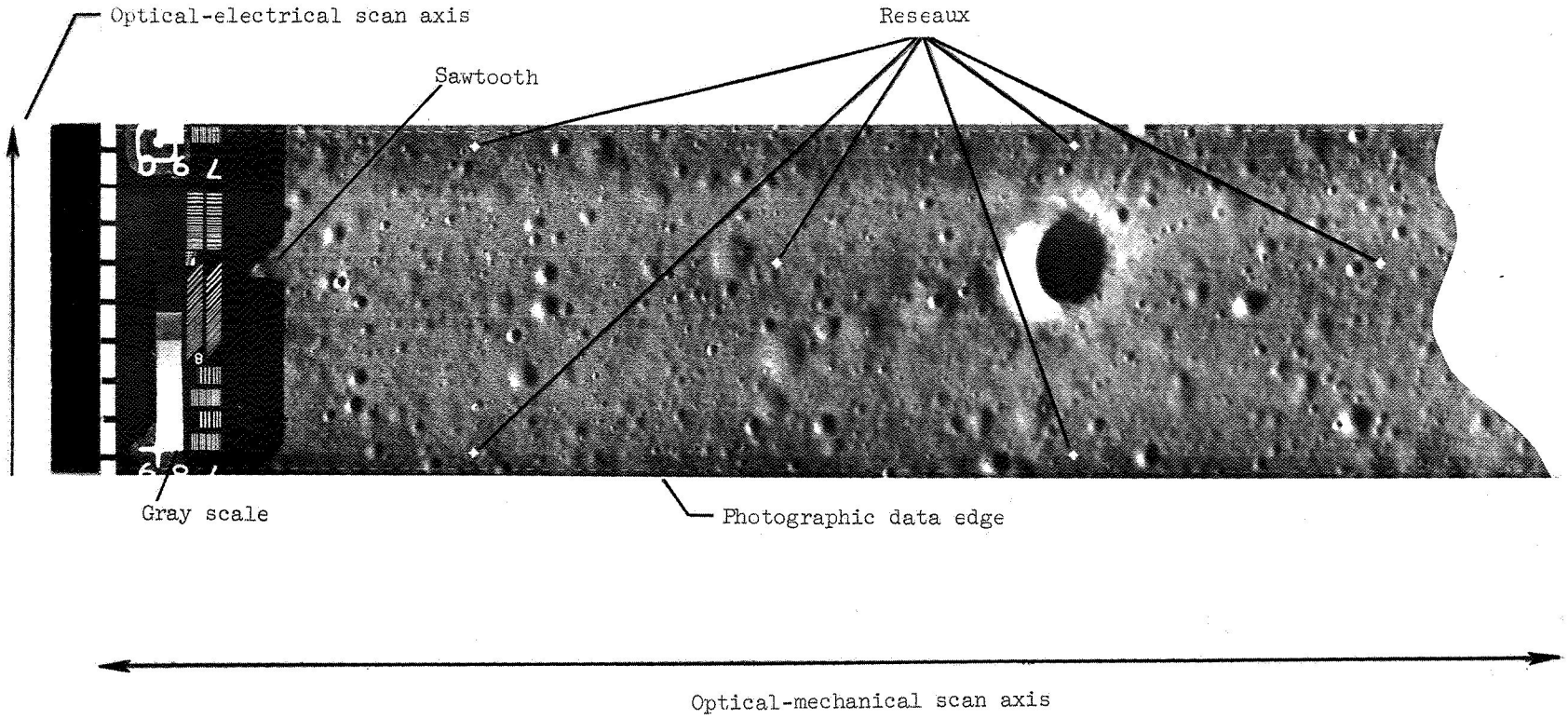

Figure 4.- Portion of a mission II framelet.

L-70-1665

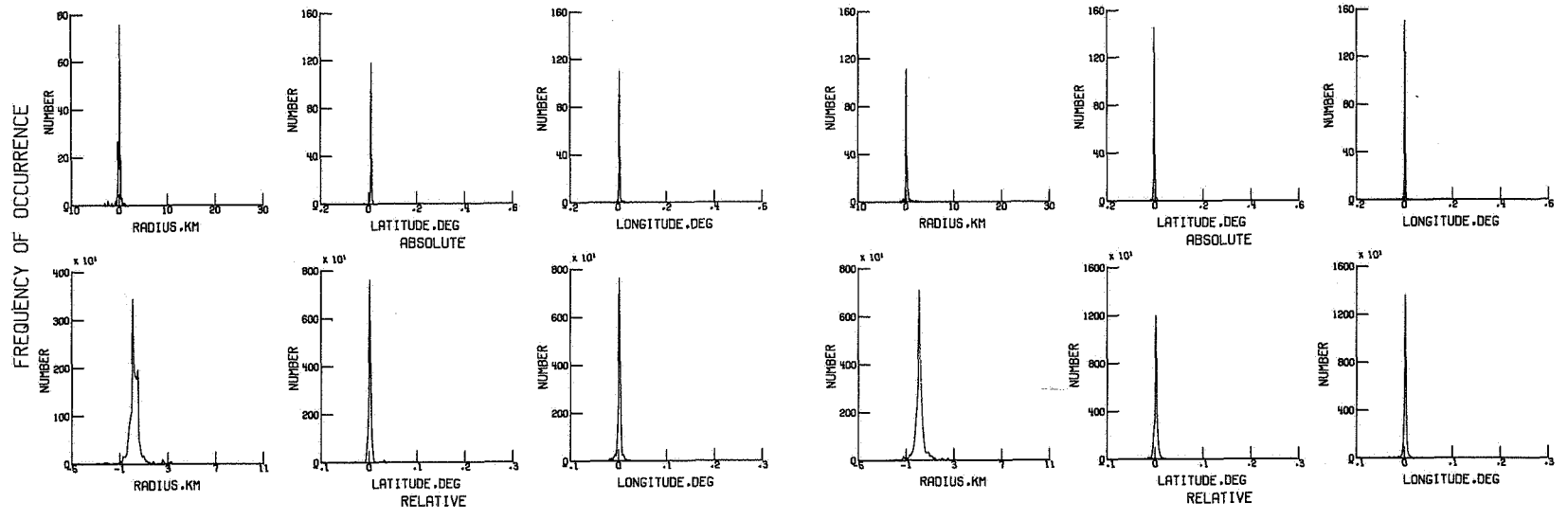

(a) II P-8BC compared with II P-8B.

(b) II P-8ABC compared with II P-8BC.

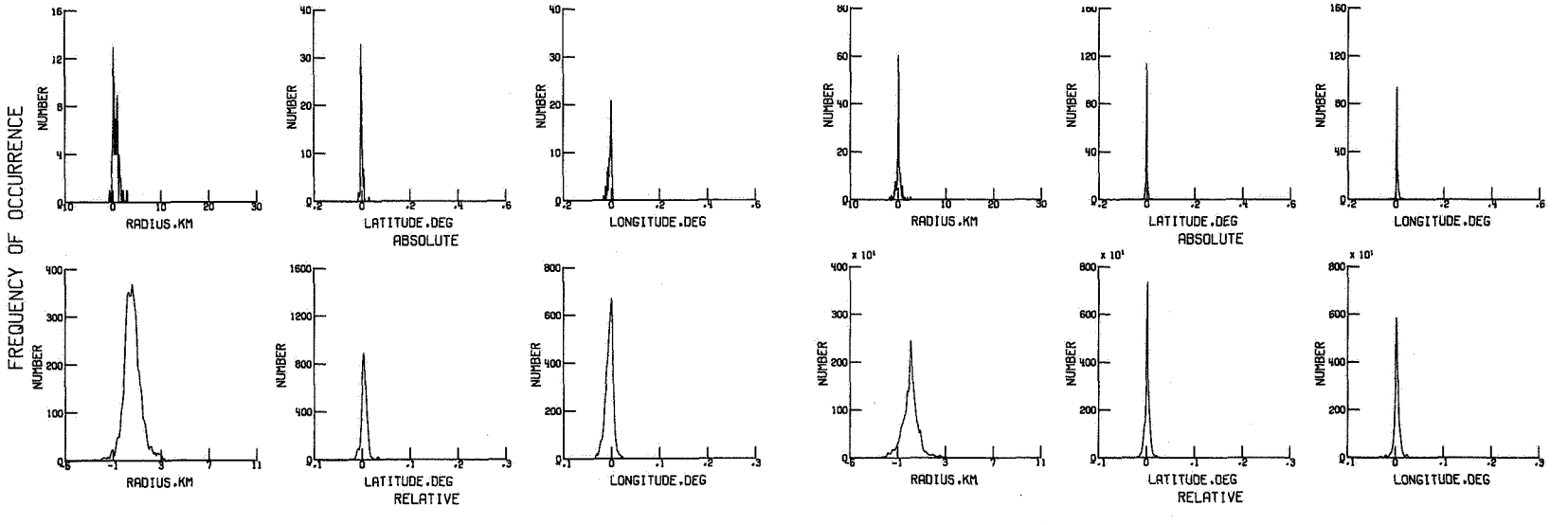

(c) II P-8B compared with II P-8C.

(d) II P-8AC compared with II P-8BC.

Figure 5.- Distribution of relative and absolute discrepancies existing between the selenographic coordinates for various combinations of strip and block solutions.

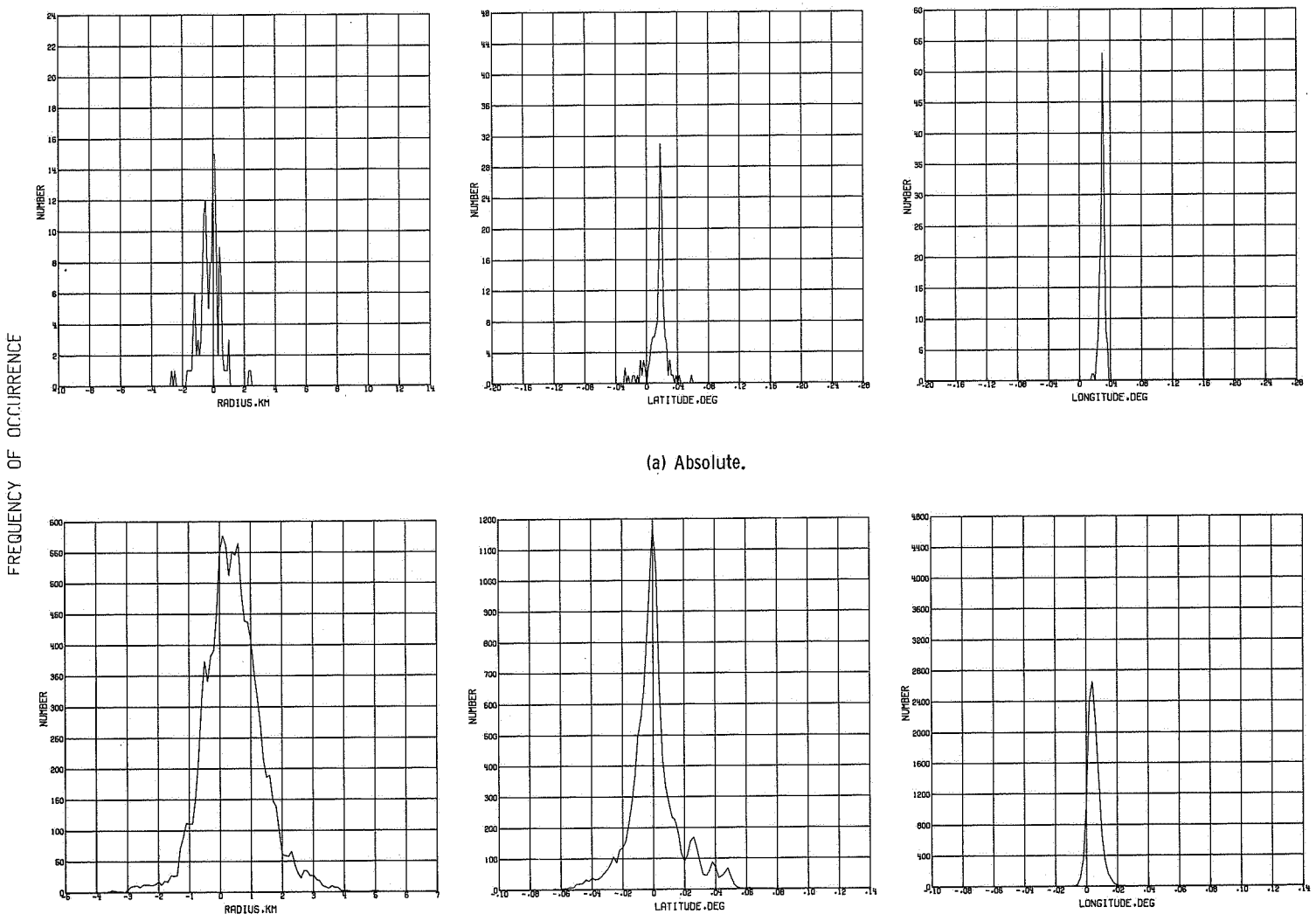

Figure 6.- Distribution of the discrepancies existing between the selenographic radii, latitudes, and longitudes for the block solution II P-8ABC and the block solution III P-7AB.

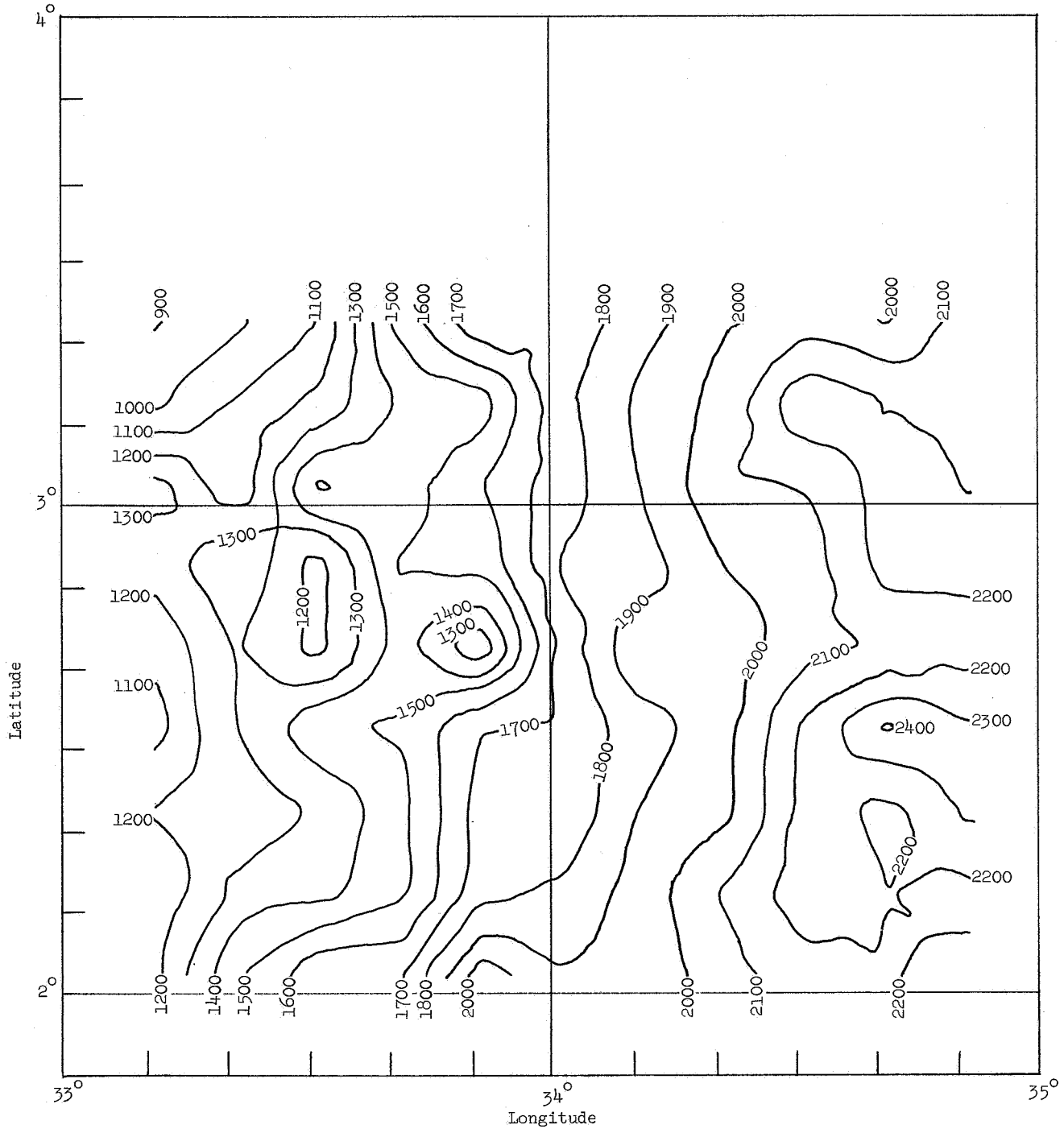

Figure 7.- A computer-generated contour chart of site II P-2 referred to as Apollo site 1. Scale: 10 min ≡ 5047 meters.

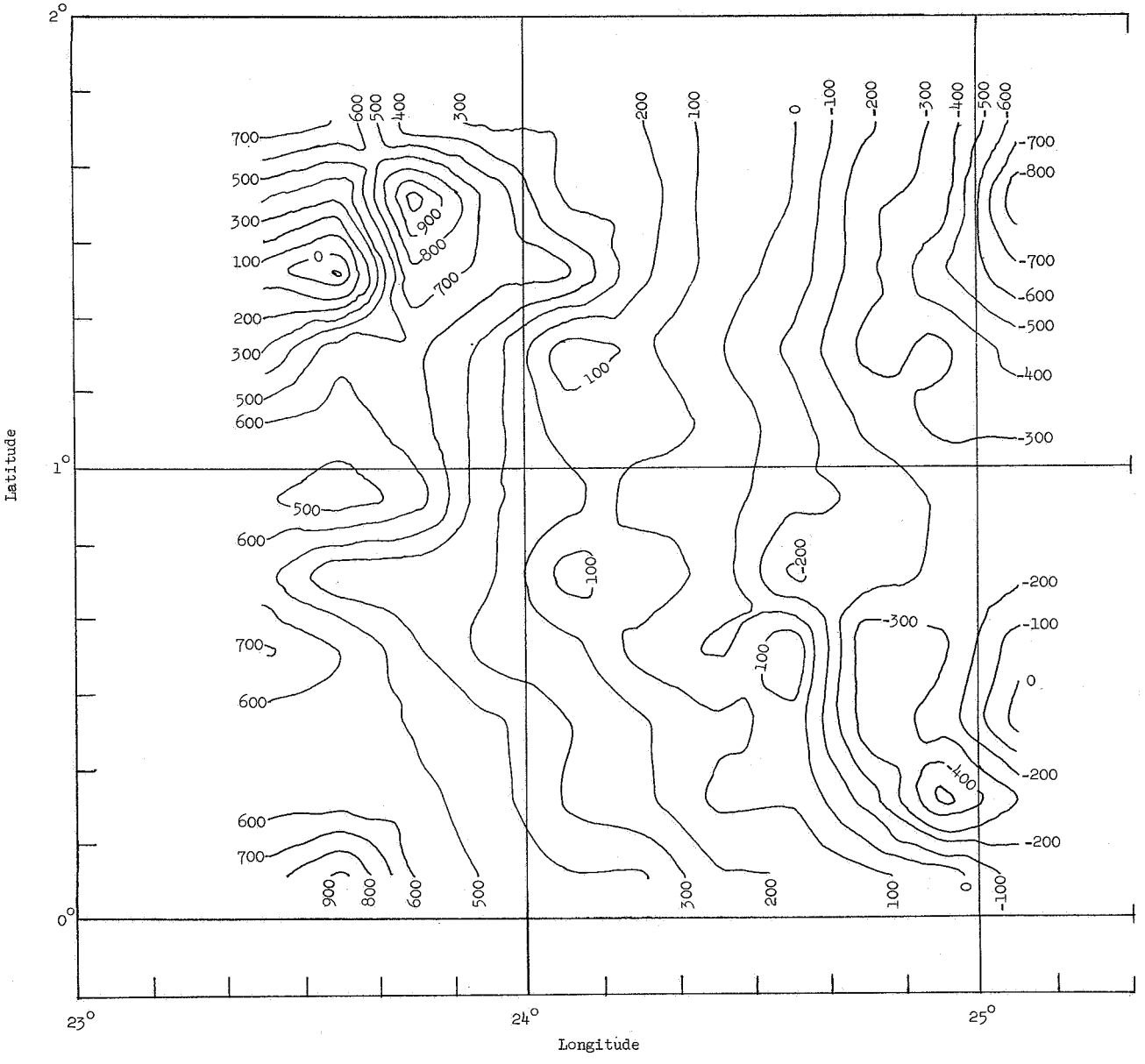

Figure 8.- A computer-generated contour chart of site II P-6AB referred to as Apollo site 2. Scale: 10 min ≡ 5047 meters.

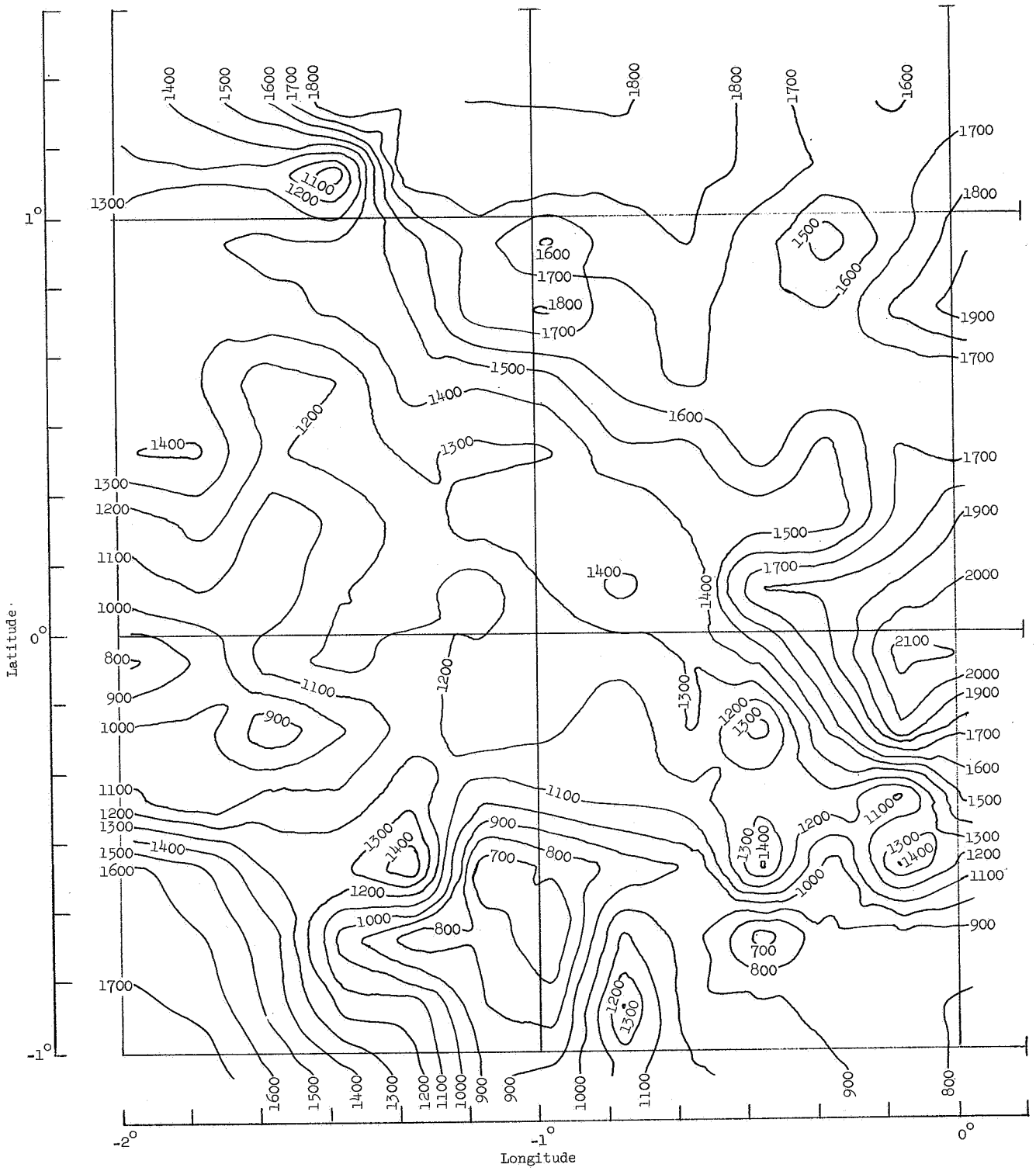

Figure 9.- A computer-generated contour chart of site II P-8ABC referred to as Apollo site 3. Scale: 10 min ≡ 5047 meters.

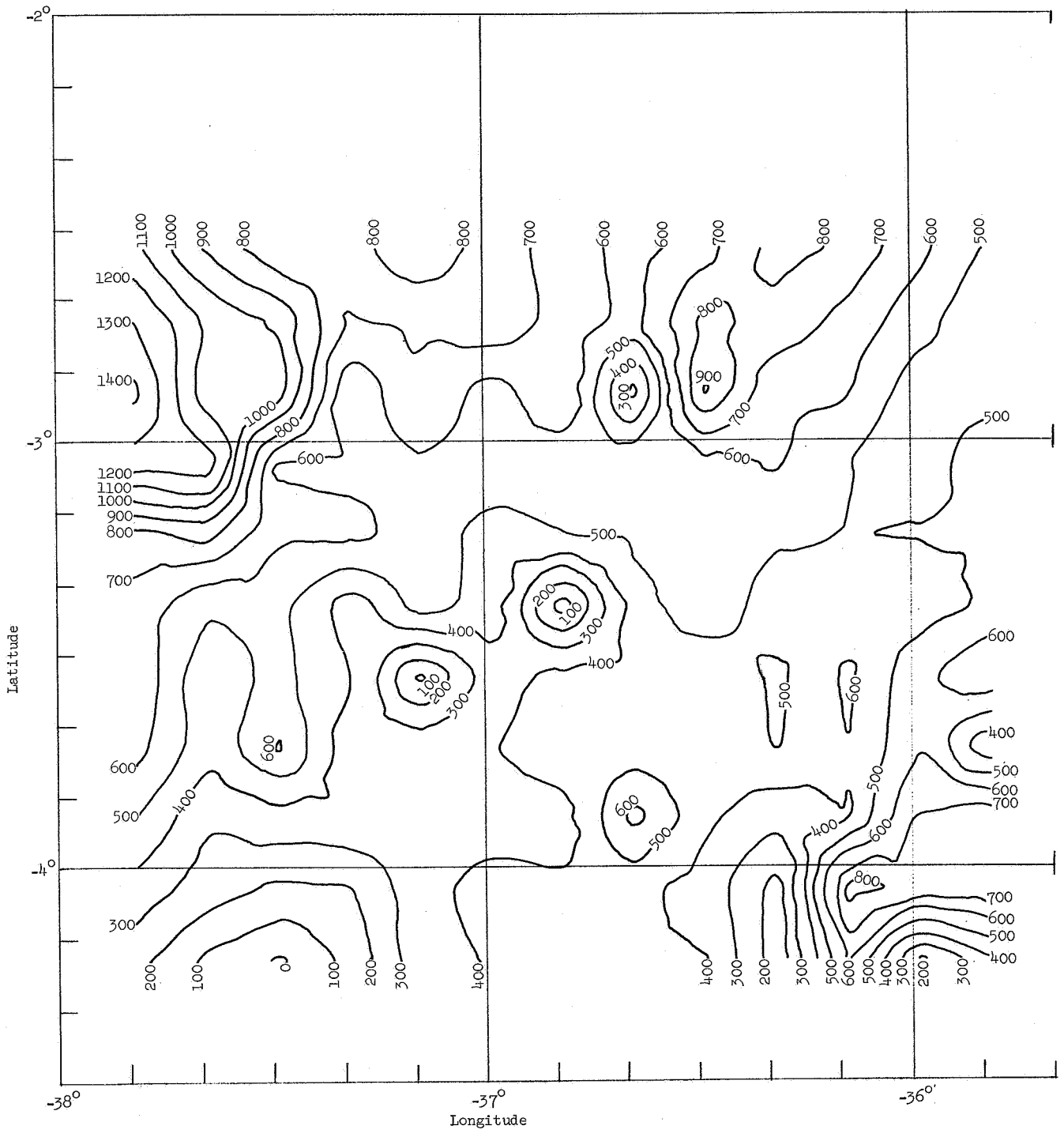

Figure 10.- A computer-generated contour chart of site III P-11 referred to as Apollo site 4. Scale: 10 min ≡ 5047 meters.

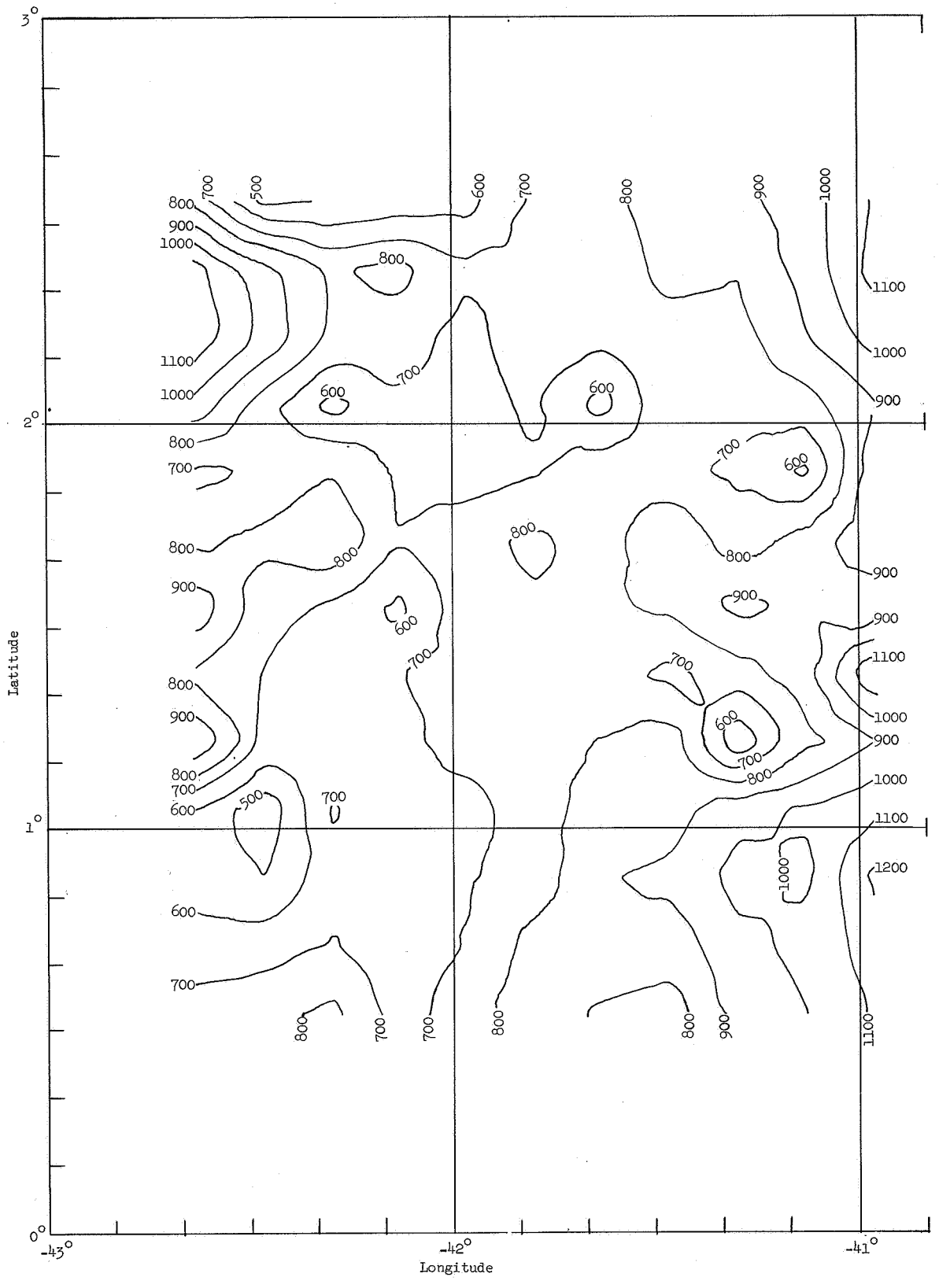

Figure 11.- A computer-generated contour chart of site II P-13AB referred to as Apollo site 5. Scale: 10 min ≡ 5047 meters.

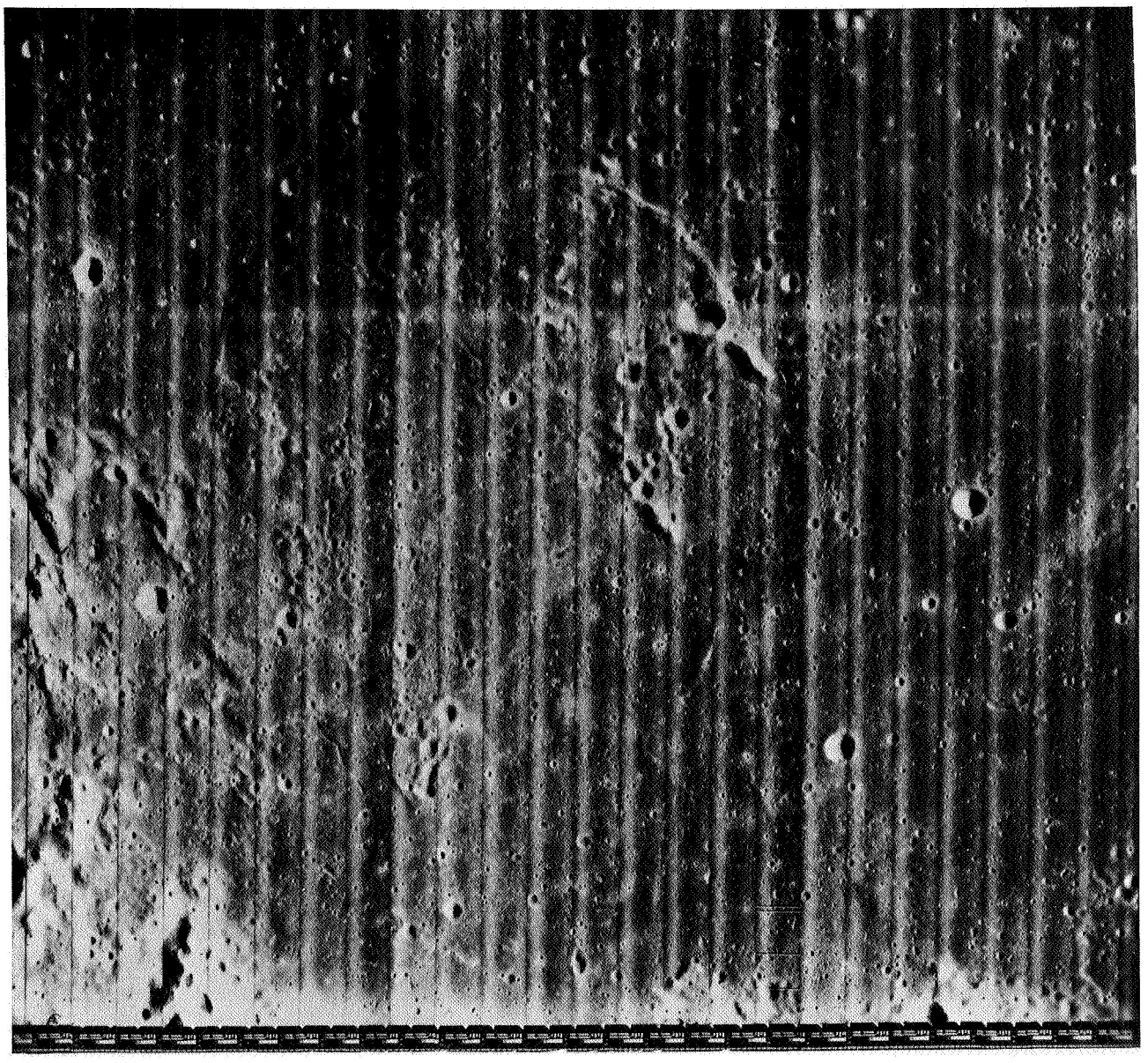

Figure 12.- Lunar Orbiter mission V moderate resolution frame number 57 covering Apollo site 1. L-70-1661

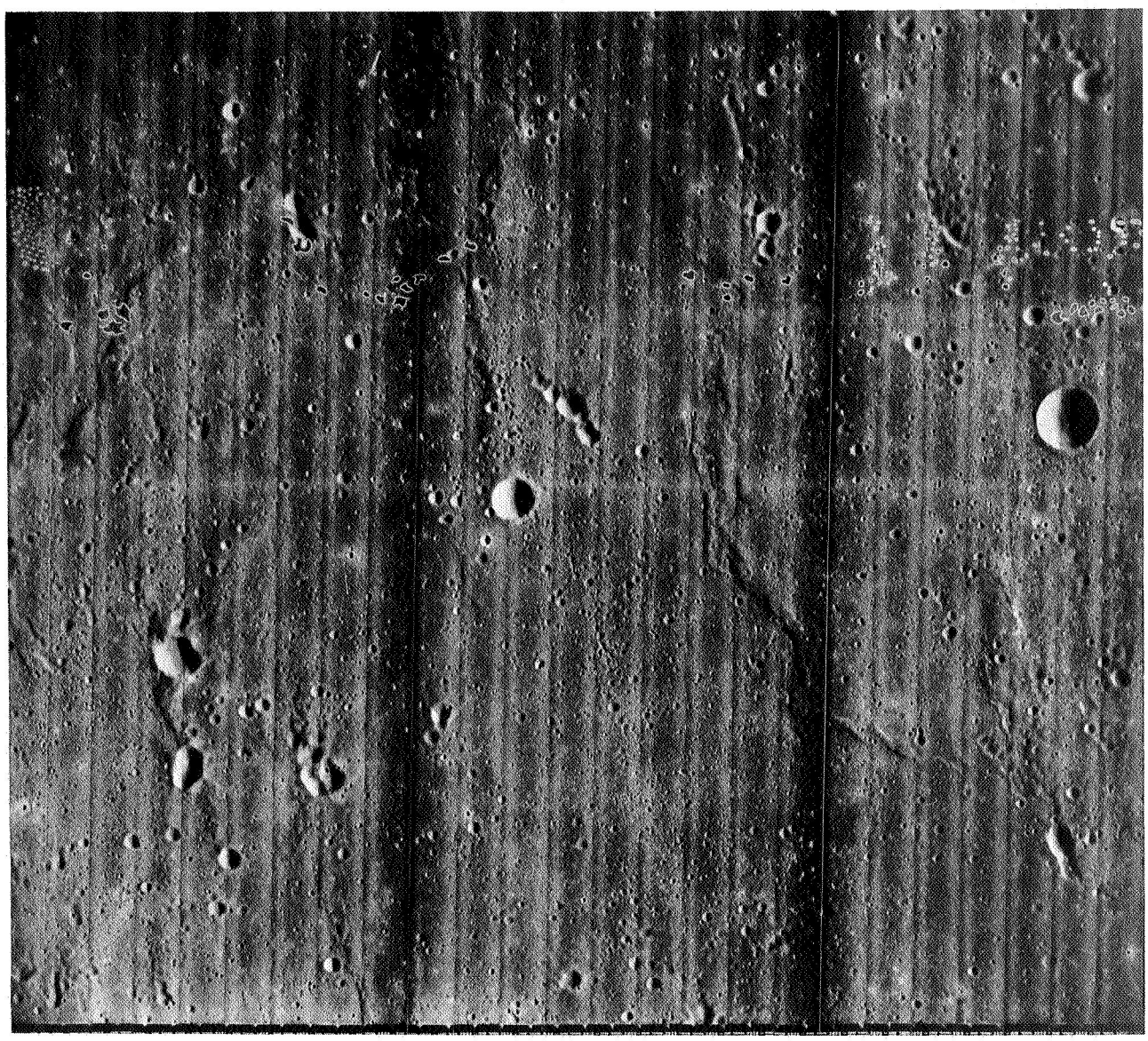

Figure 13.- Lunar Orbiter mission V moderate resolution frame number 74 covering Apollo site 2. L-70-1662

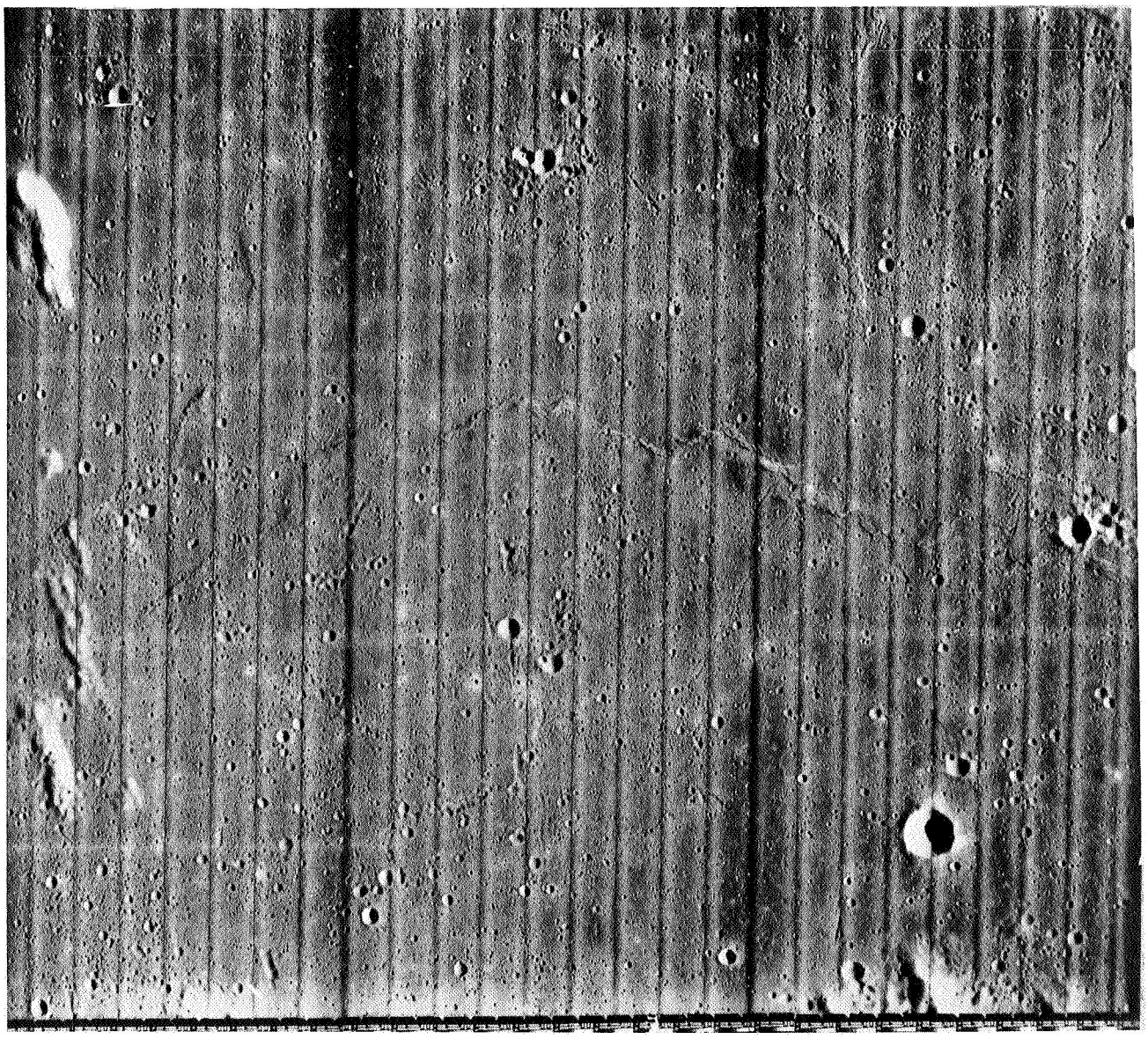

Figure 14.- Lunar Orbiter mission V moderate resolution frame number 109 covering Apollo site 3. L-70-1663

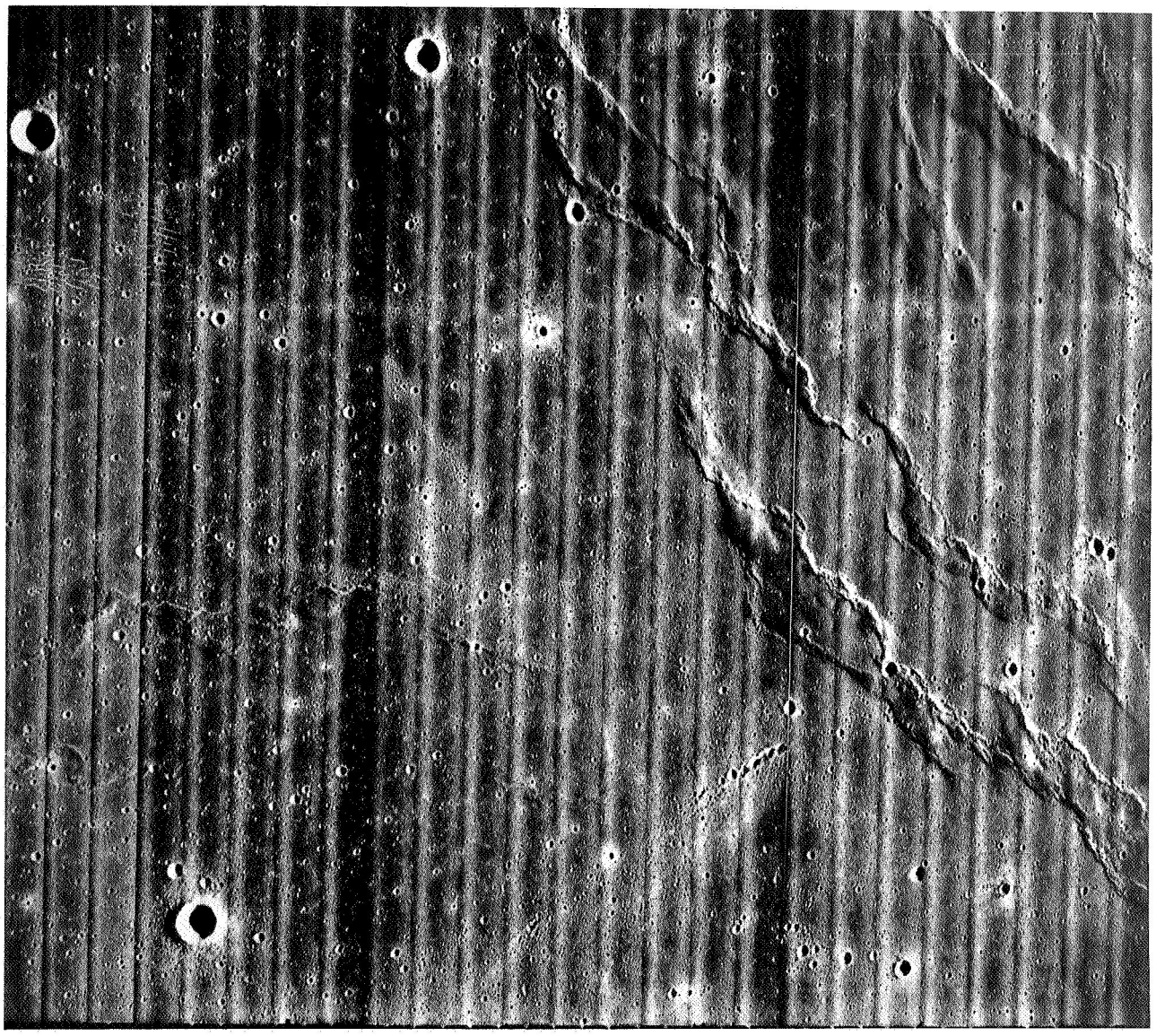

Figure 15.- Lunar Orbiter mission V moderate resolution frame number 173 covering Apollo site 4. L-70-1664

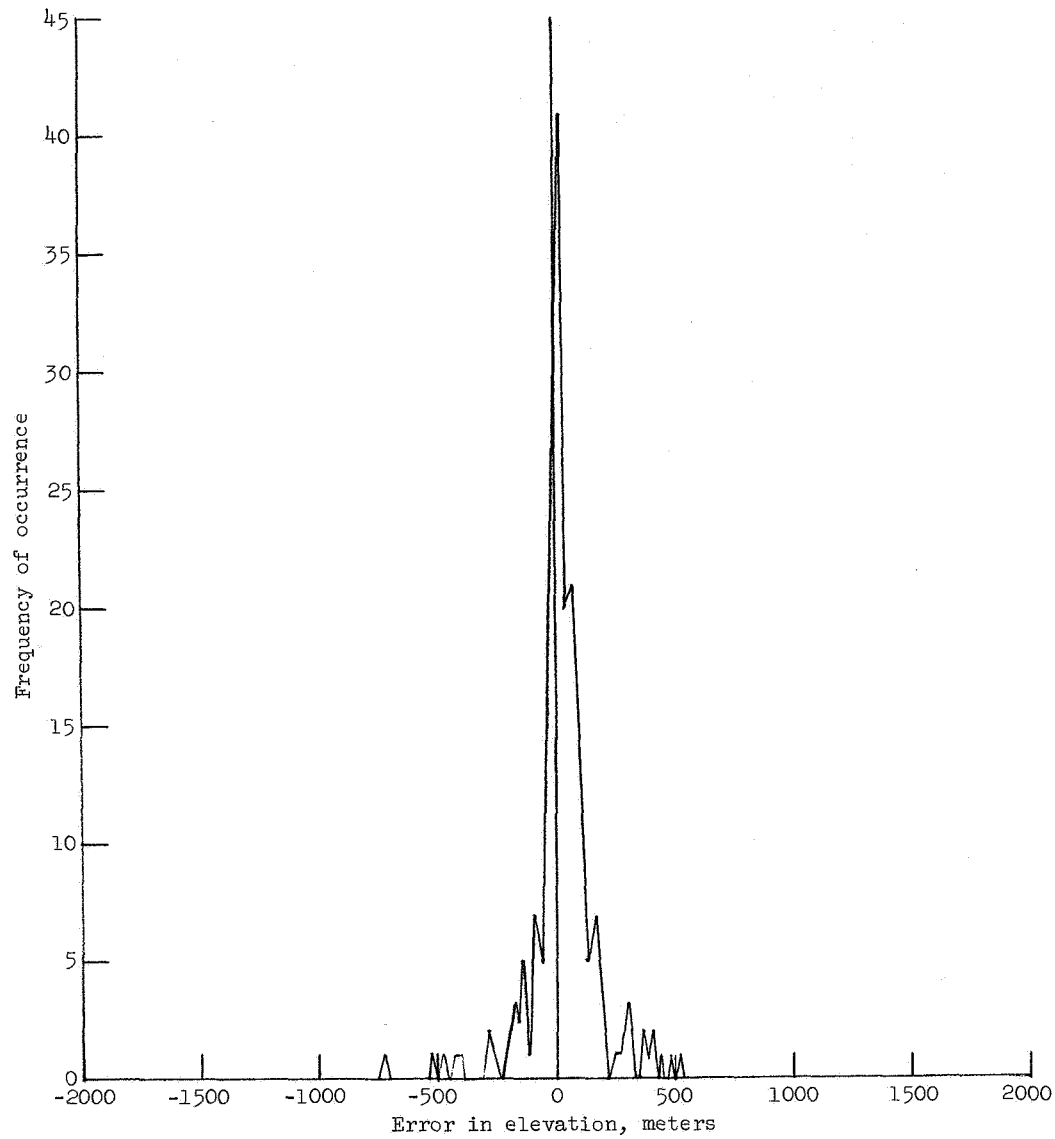

Figure 16.- Frequency distribution of differences existing between the elevation of a feature and its value predicted by the depth matrix for the contour chart of site I P-5.

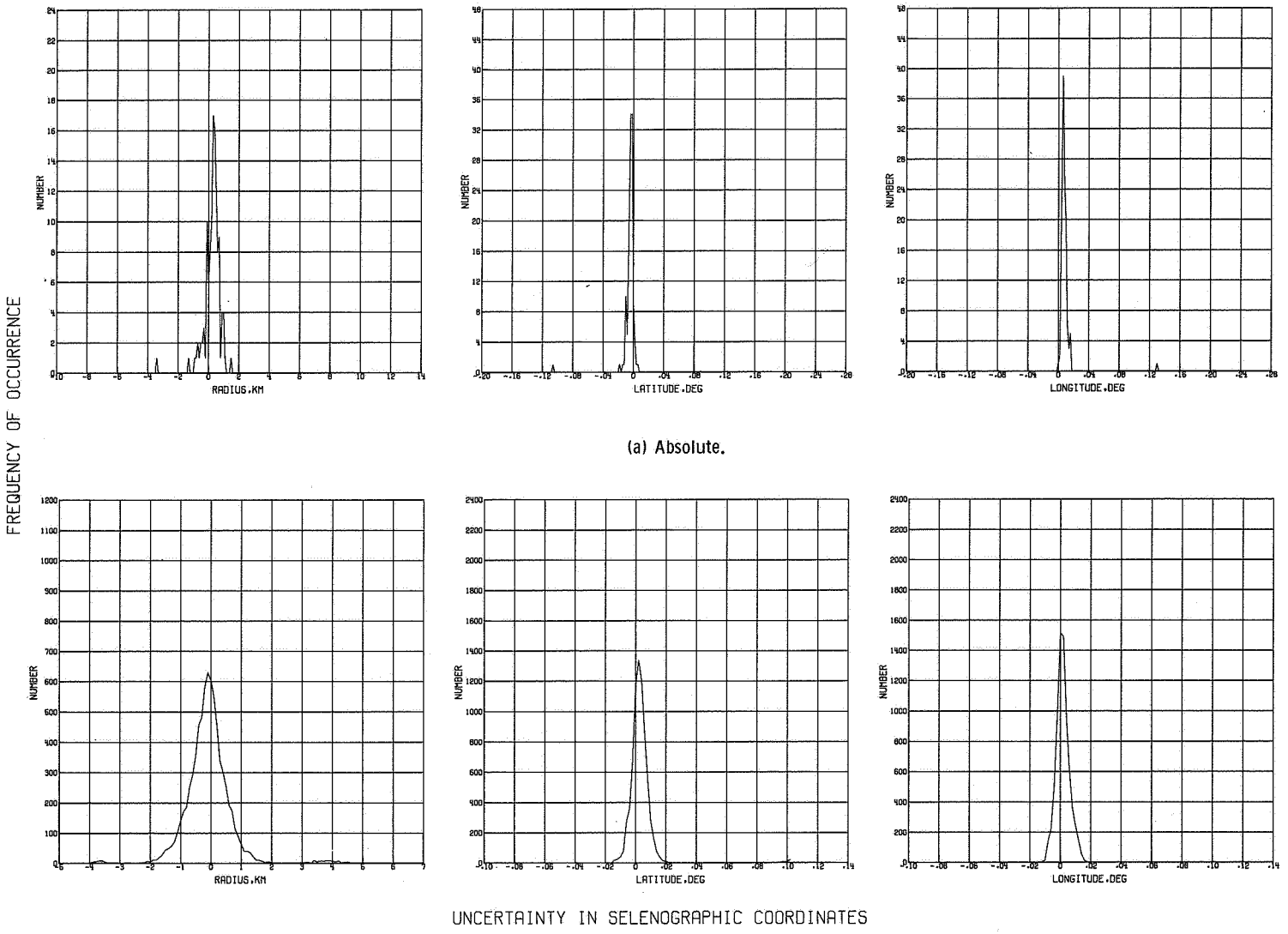

Figure 17.- Distribution of the discrepancies existing between the selenographic radii, latitudes, and longitudes for the strip solution II P-8A and the strip solution II P-8B.

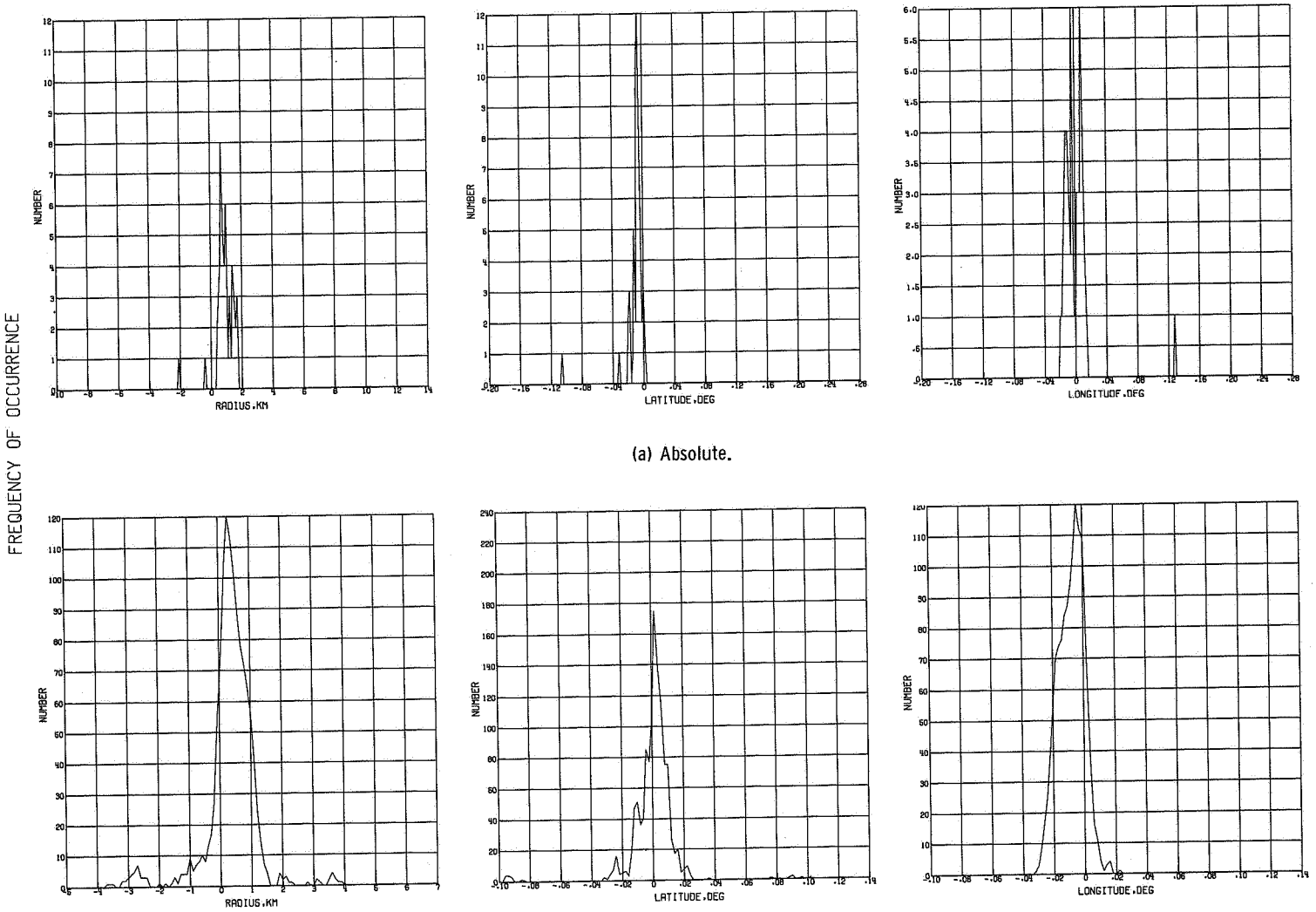

(a) Absolute.

(b) Relative.

Figure 18.- Distribution of the discrepancies existing between the selenographic radii, latitudes, and longitudes for the strip solution II P-8A and the strip solution II P-8C.

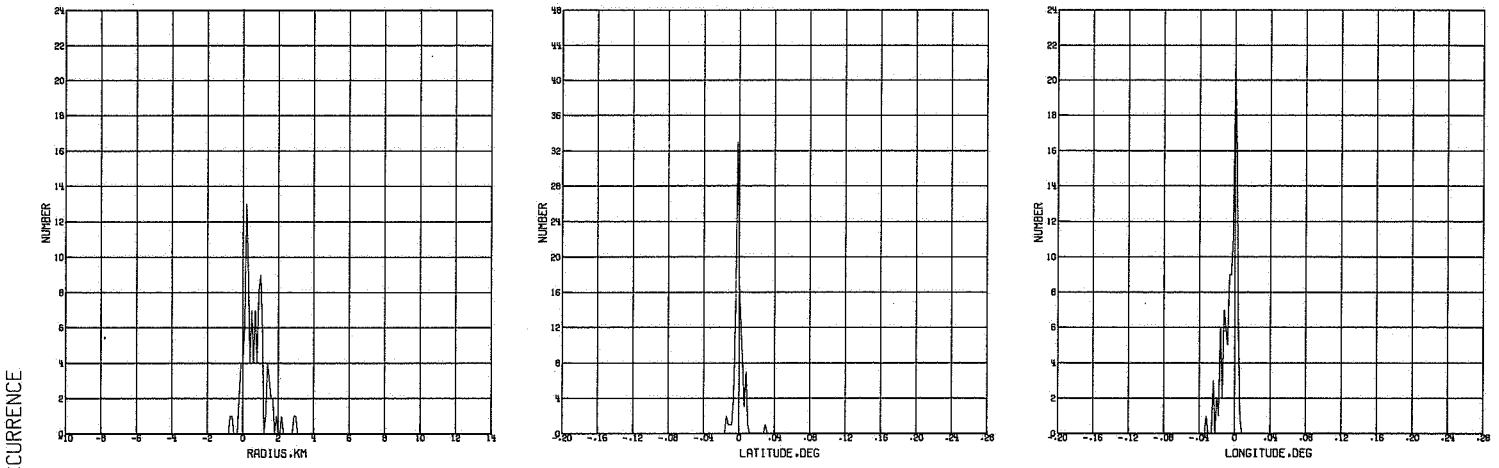

(a) Absolute.

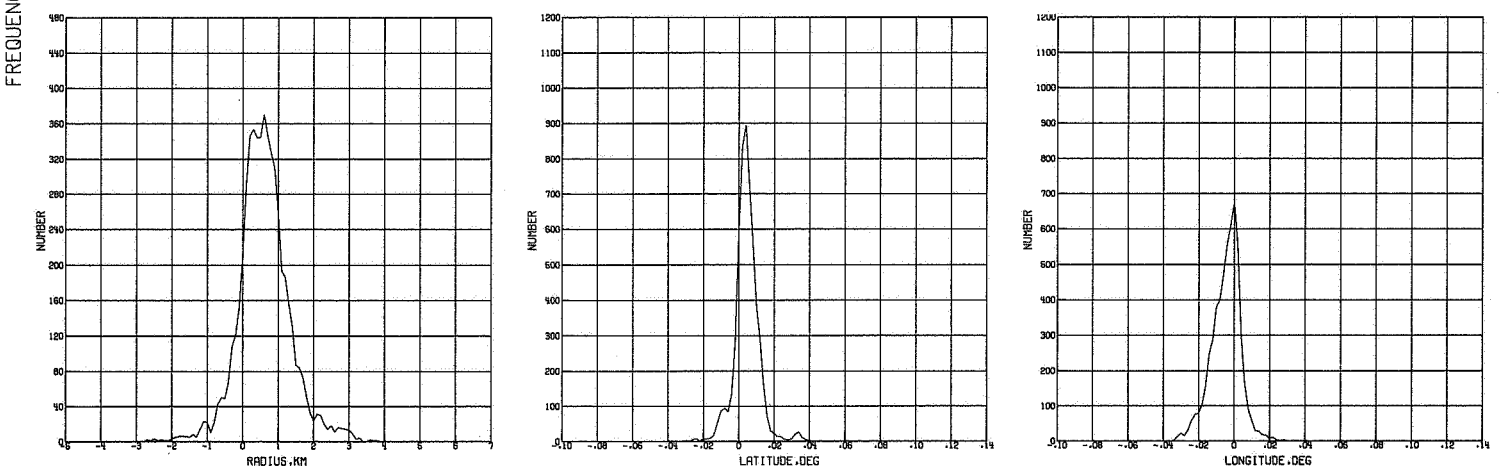

(b) Relative.

Figure 19.- Distribution of the discrepancies existing between the selenographic radii, latitudes, and longitudes for the strip solution II P-8B and the strip solution II P-8C.

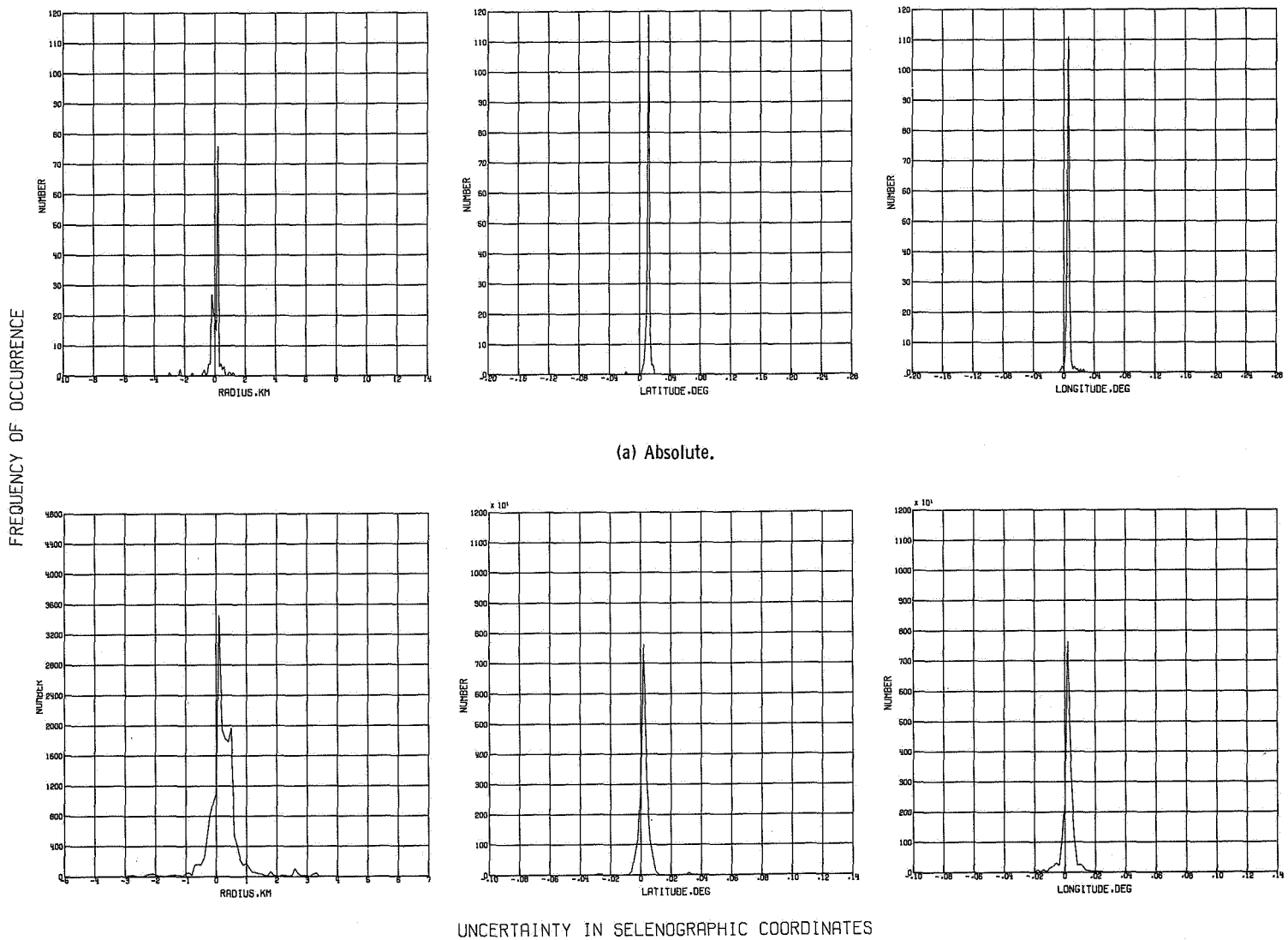

(a) Absolute.

(b) Relative.

Figure 20.- Distribution of the discrepancies existing between the selenographic radii, latitudes, and longitudes for the block solution II P-8BC and the strip solution II P-8B.

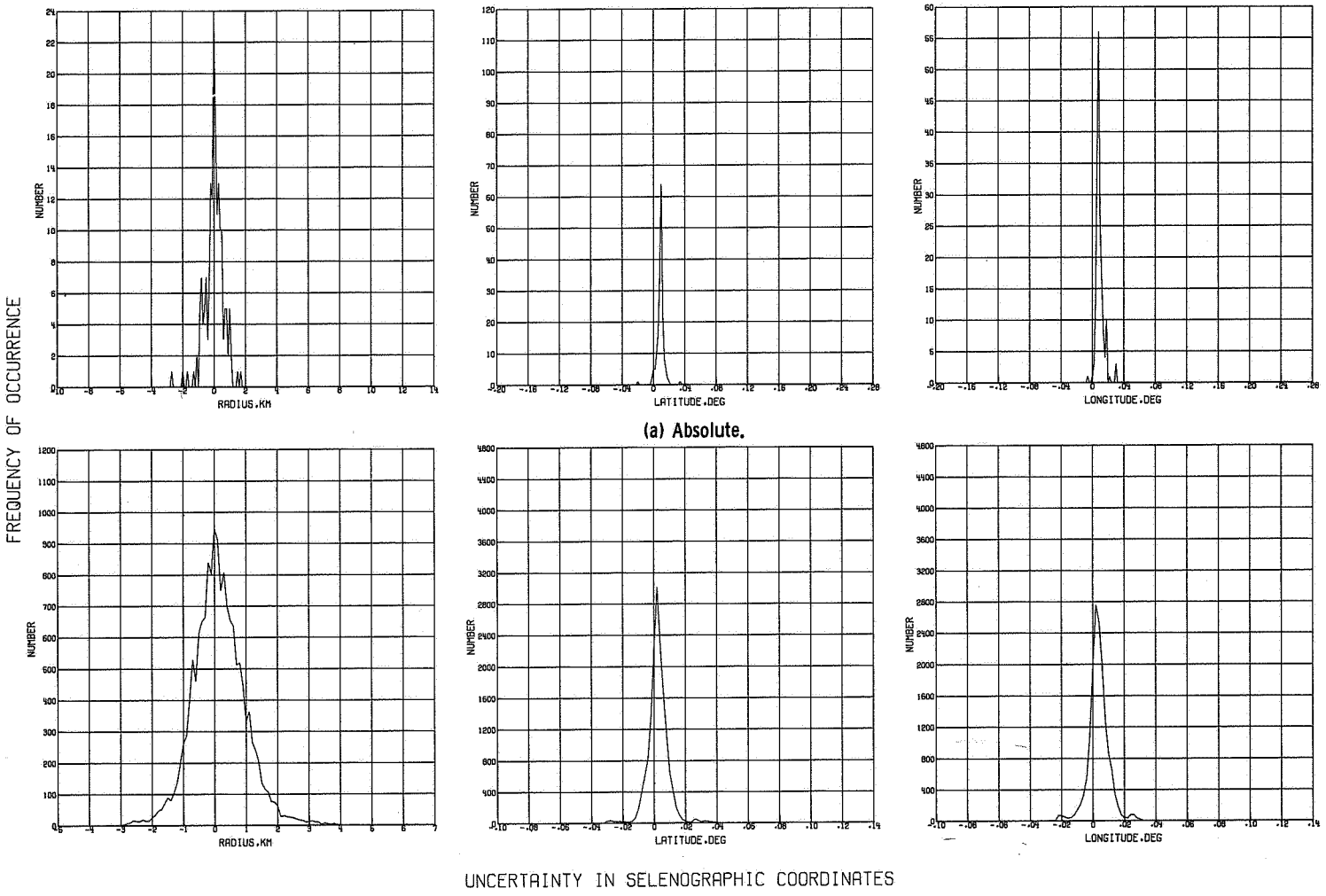

Figure 21.- Distribution of the discrepancies existing between the selenographic radii, latitudes, and longitudes for the block solution II P-8AC and the strip solution II P-8B.

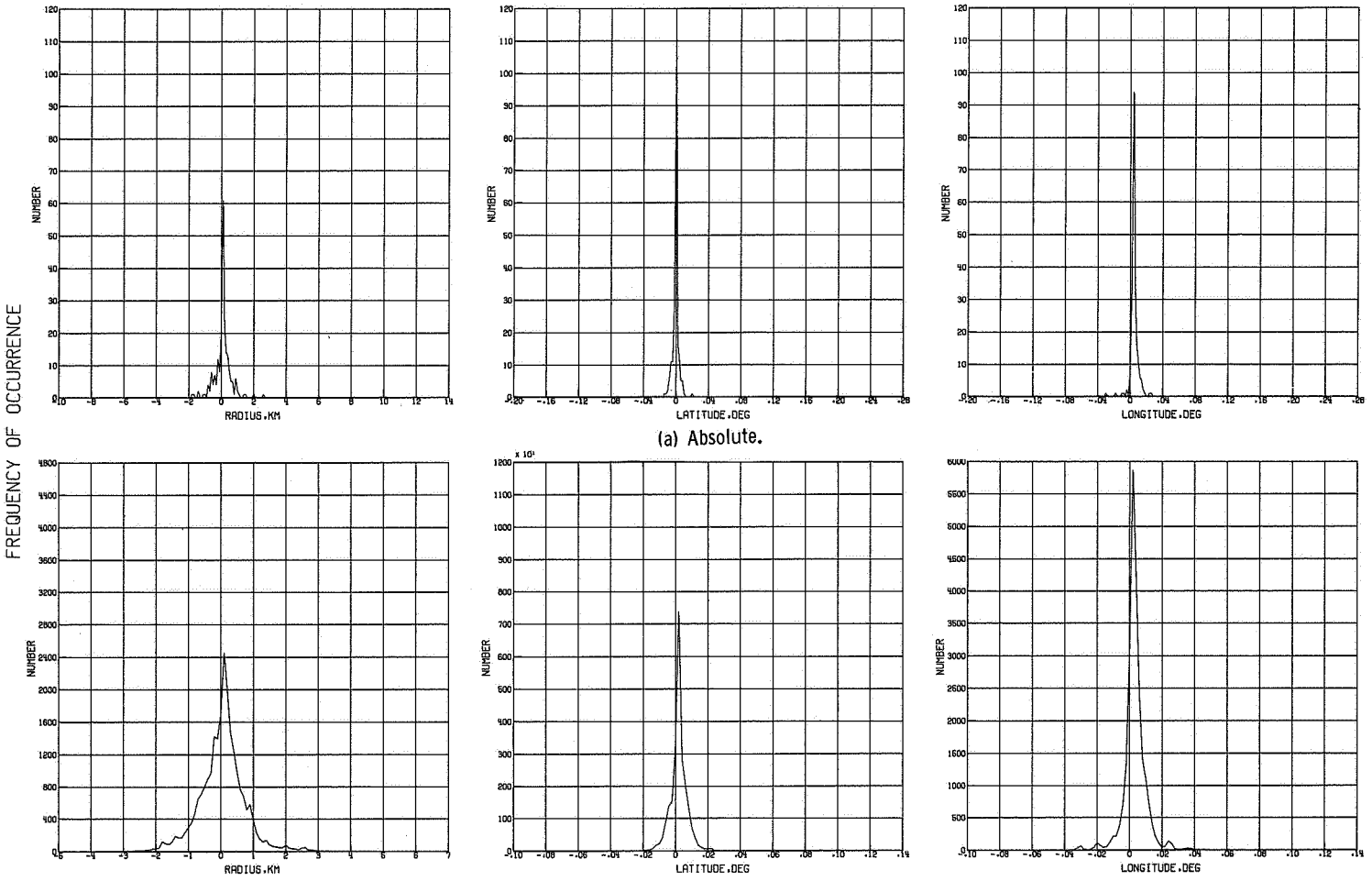

Figure 22.- Distribution of the discrepancies existing between the selenographic radii, latitudes, and longitudes for the block solution II P-8AC and the block solution II P-8BC.

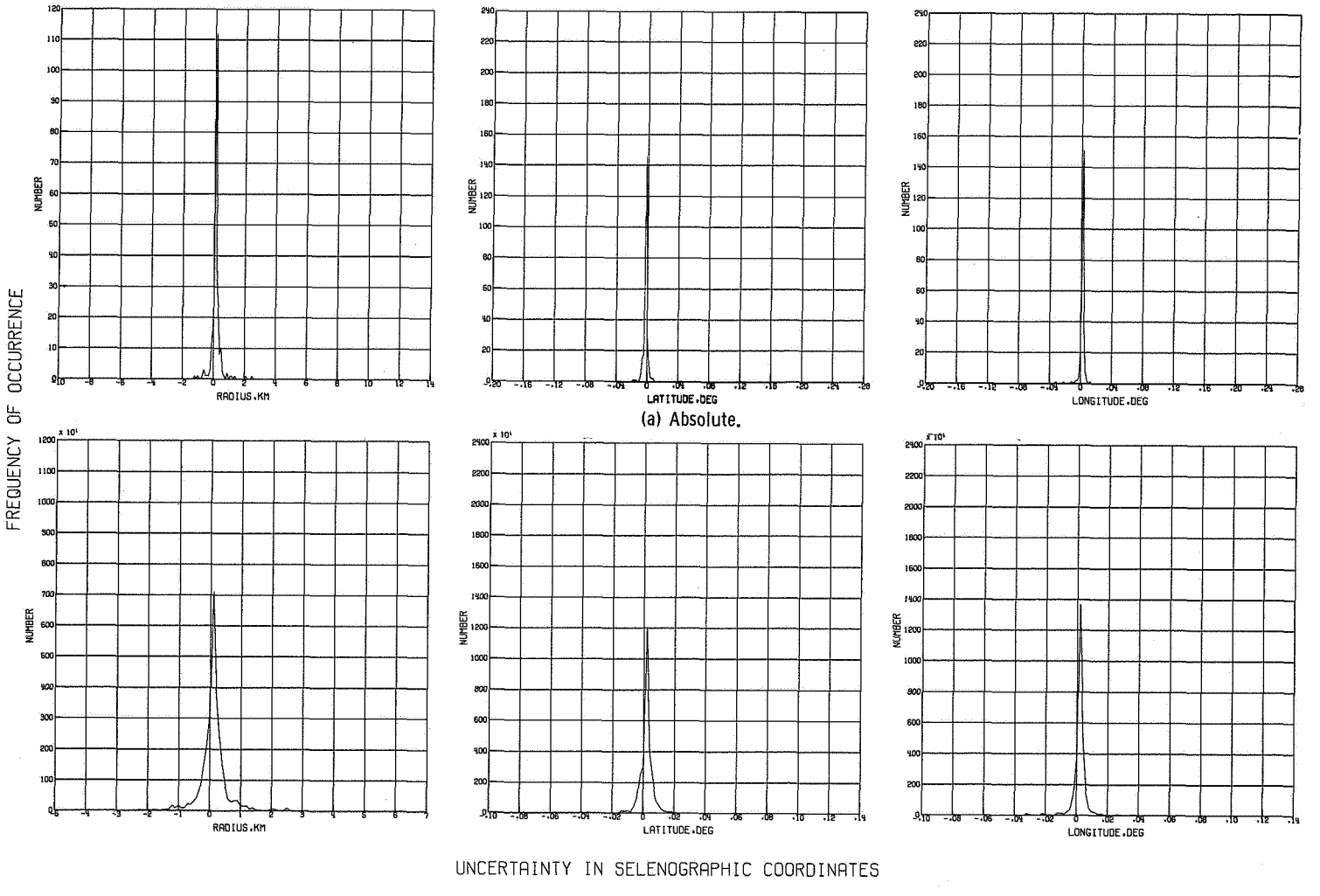

Figure 23.- Distribution of the discrepancies existing between the selenographic radii, latitudes, and longitudes for the block solution II P-8ABC and the block solution II P-8BC.

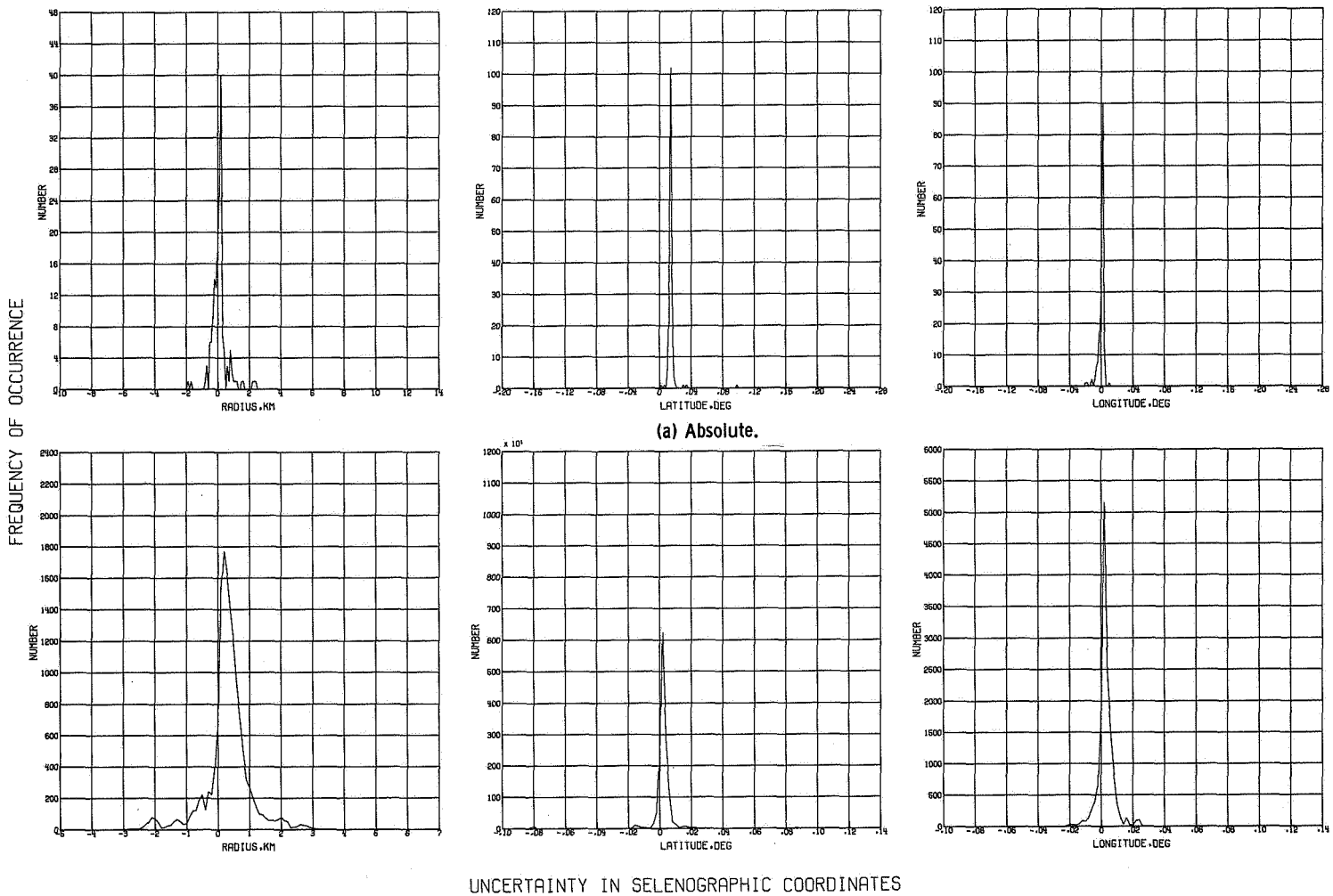

Figure 24.- Distribution of the discrepancies existing between the selenographic radii, latitudes, and longitudes for the block solution II P-8ABC and the strip solution II P-8A.

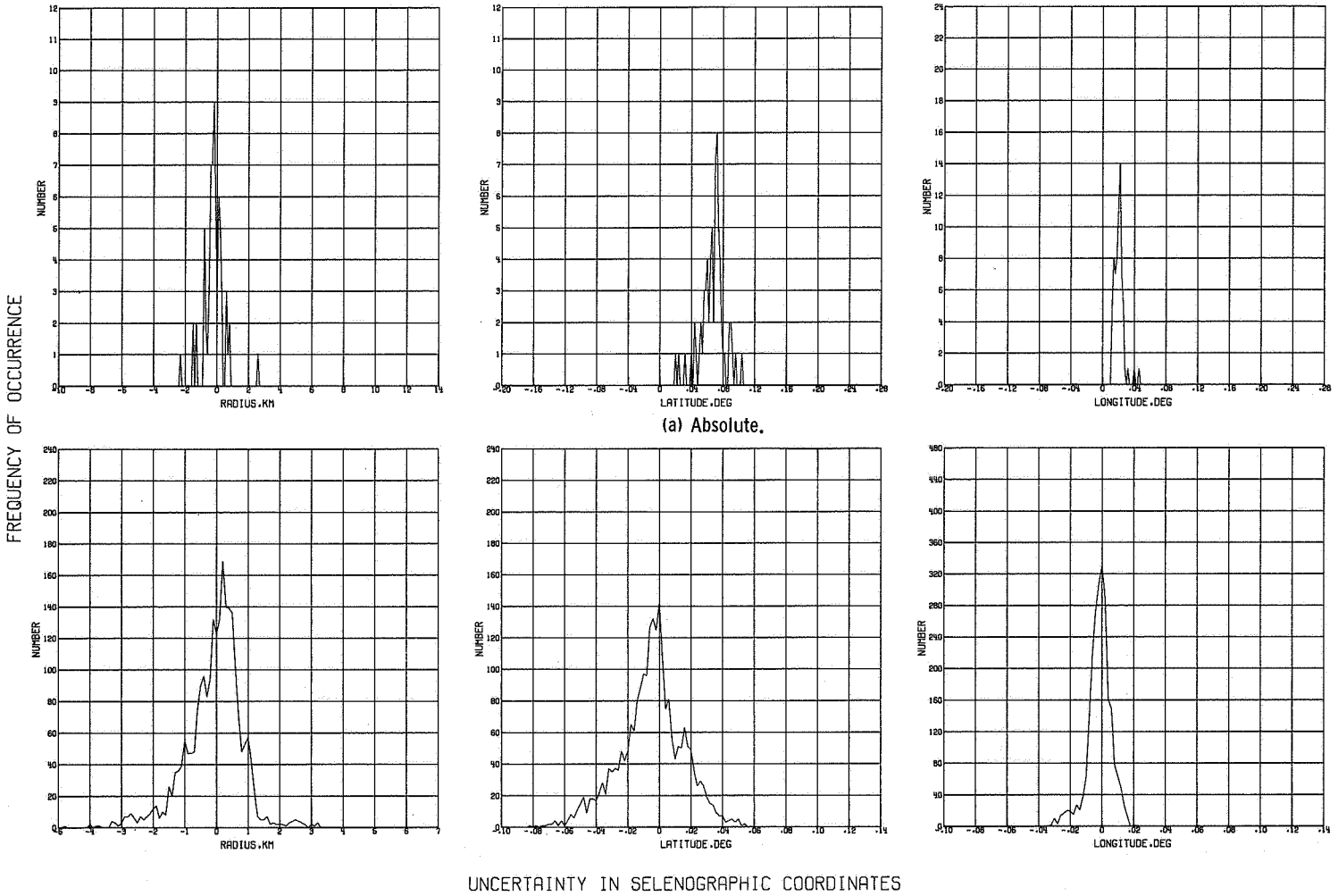

Figure 25.- Distribution of the discrepancies existing between the selenographic radii, latitudes, and longitudes for the strip solution I P-5 and the block solution III P-7AB.

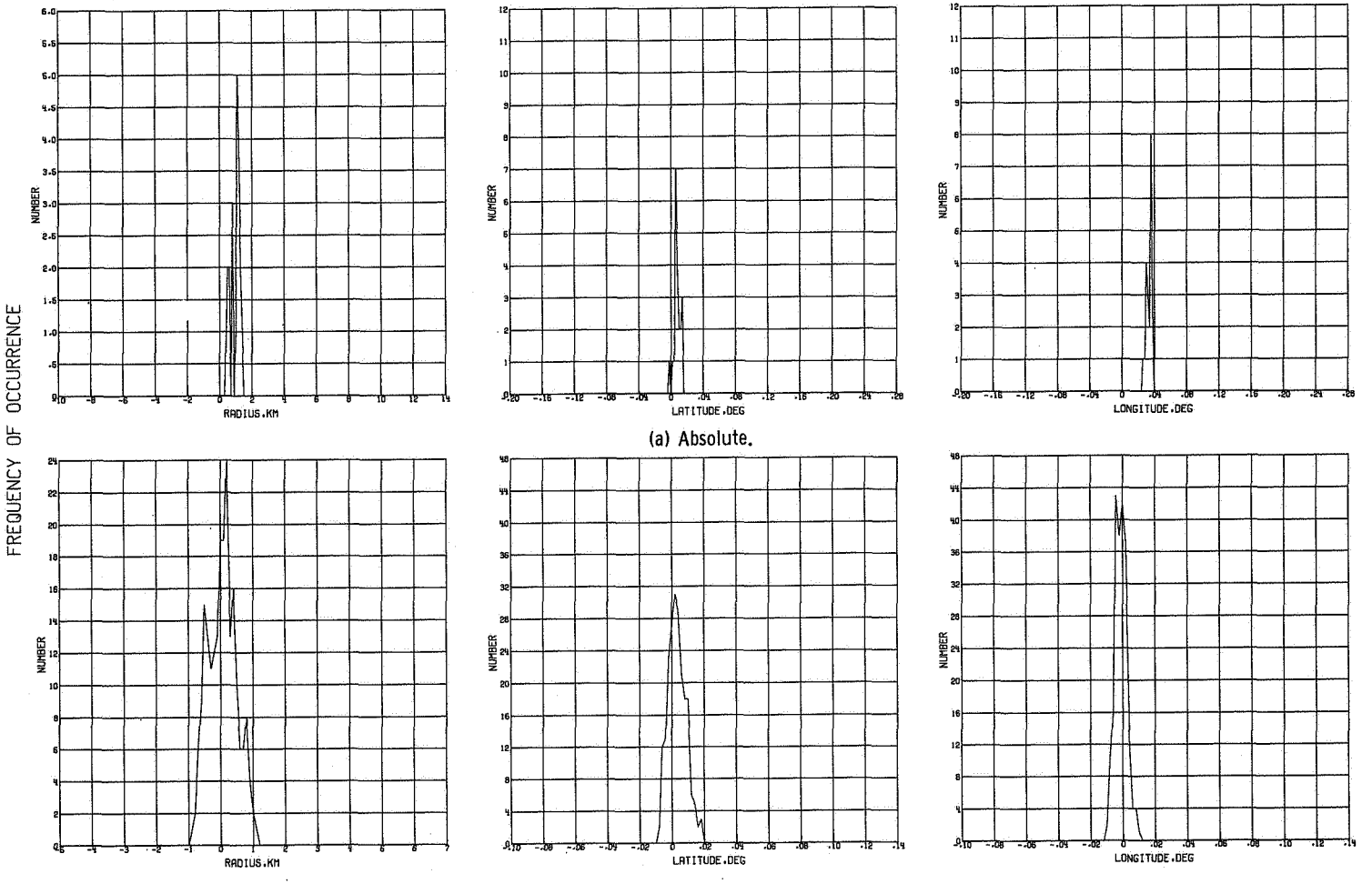

Figure 26.- Distribution of the discrepancies existing between the selenographic radii, latitudes, and longitudes for the block solution III P-7AB and the block solution II P-7AB.

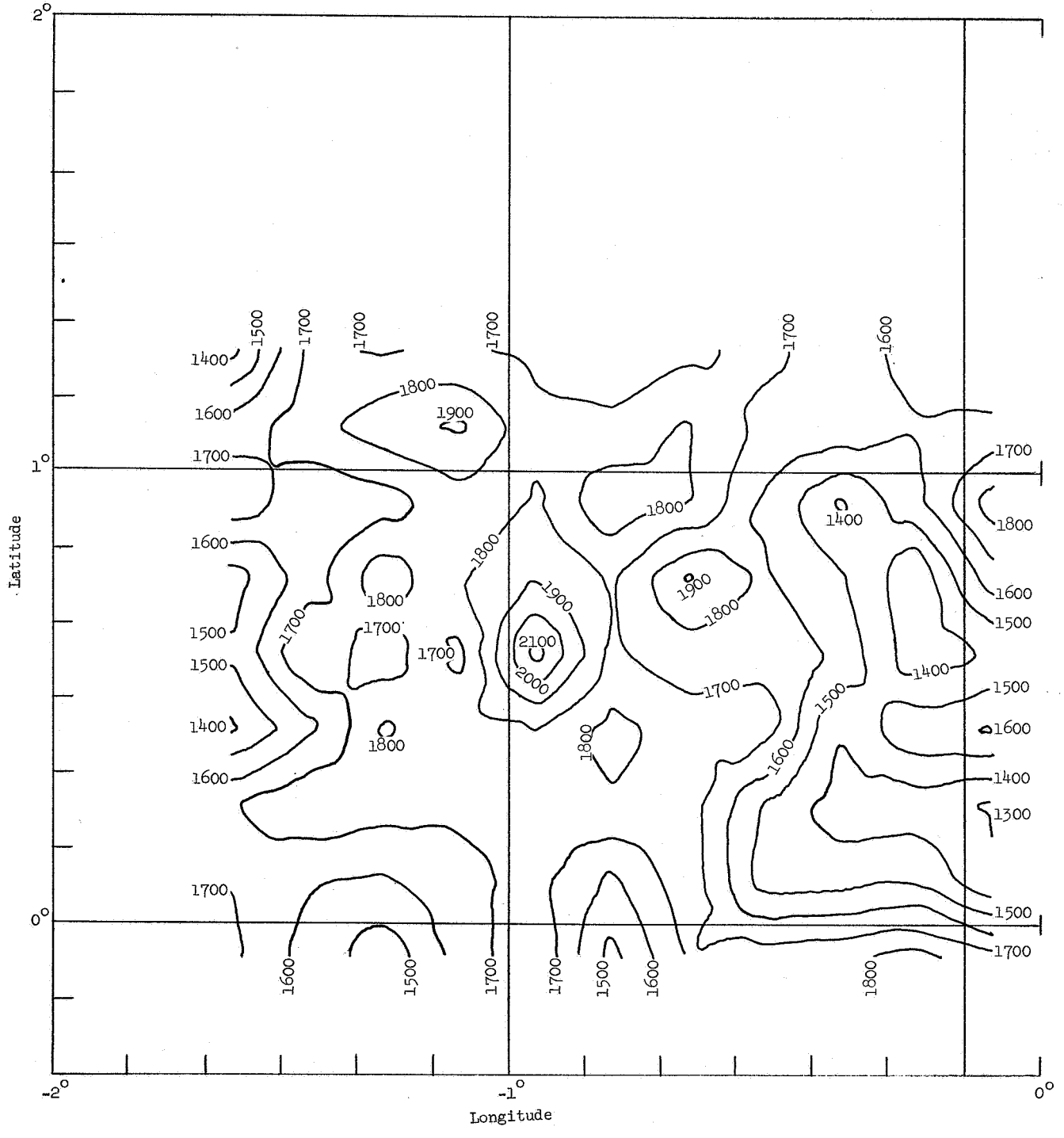

Figure 27.- A computer-generated contour chart of site II P-8A. Scale: 10 min ≡ 5047 meters.

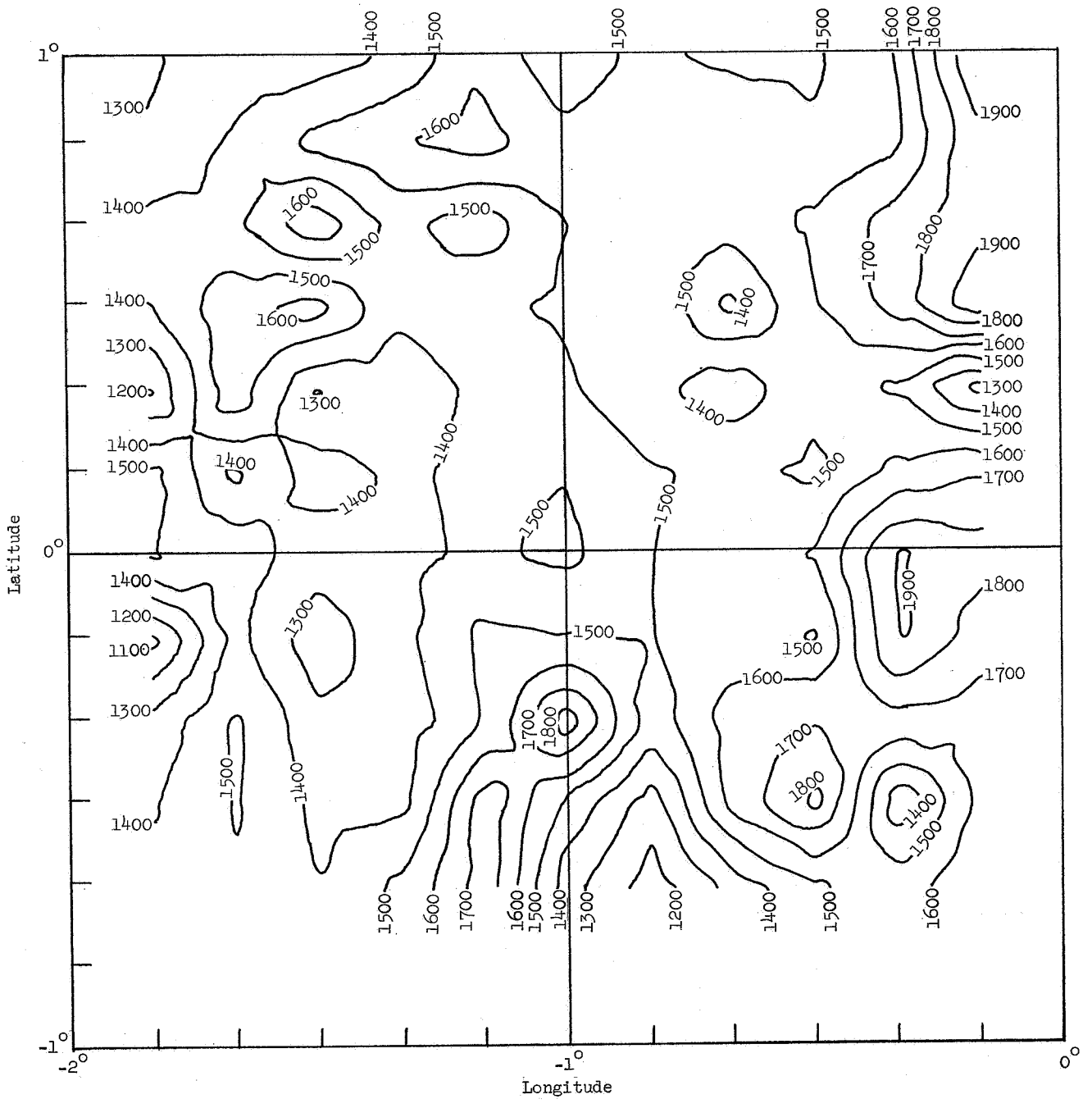

Figure 28.- A computer-generated contour chart of site II P-8B. Scale: 10 min ≡ 5047 meters.

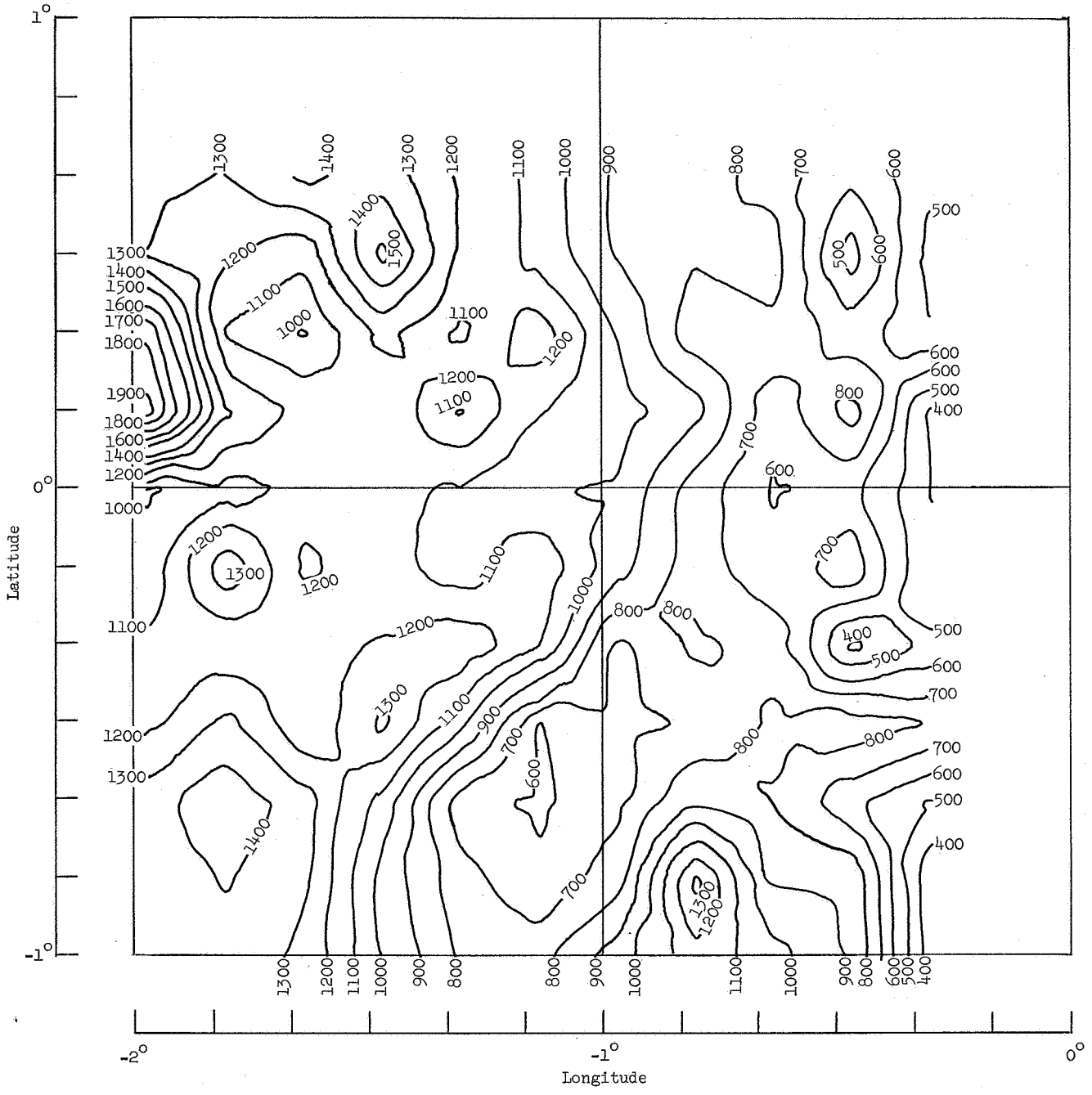

Figure 29.- A computer-generated contour chart of site II P-8C. Scale: 10 min ≡ 5047 meters.

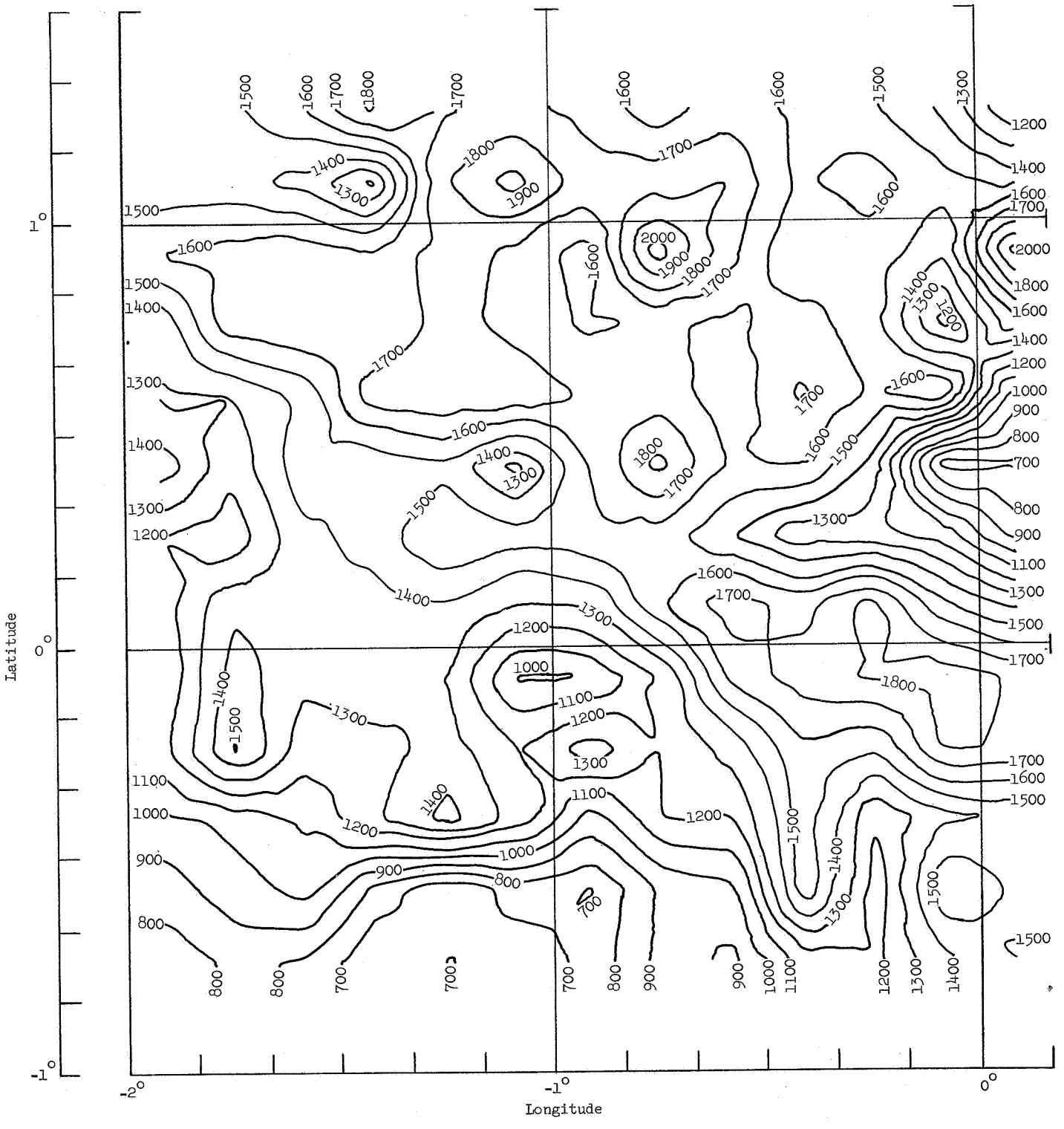

Figure 30.- A computer-generated contour chart of sites II P-8A, II P-8B, and II P-8C. Scale: 10 min ≡ 5047 meters.

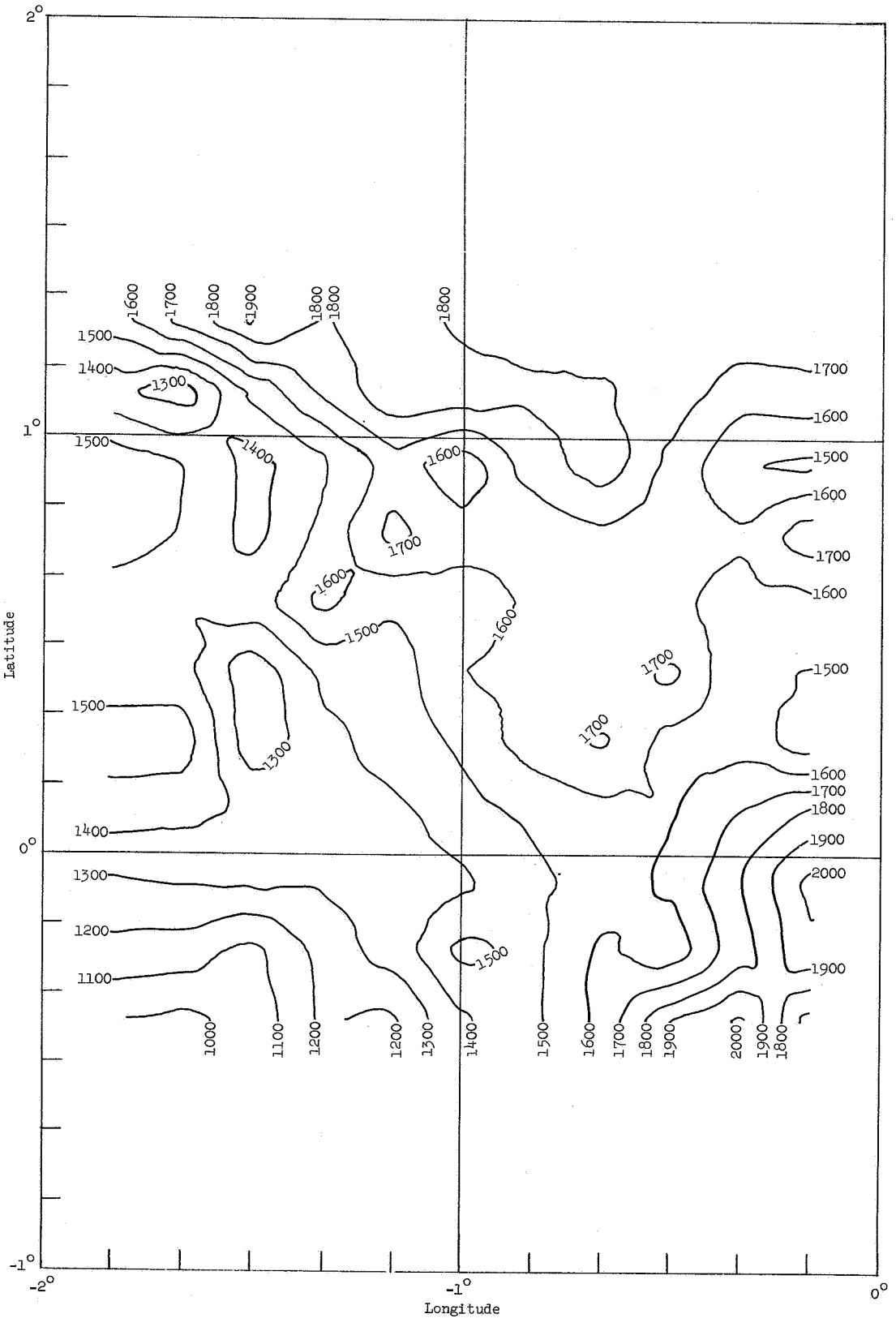

Figure 31.- A computer-generated contour chart of site II P-8AB. Scale: 10 min ≡ 5047 meters.

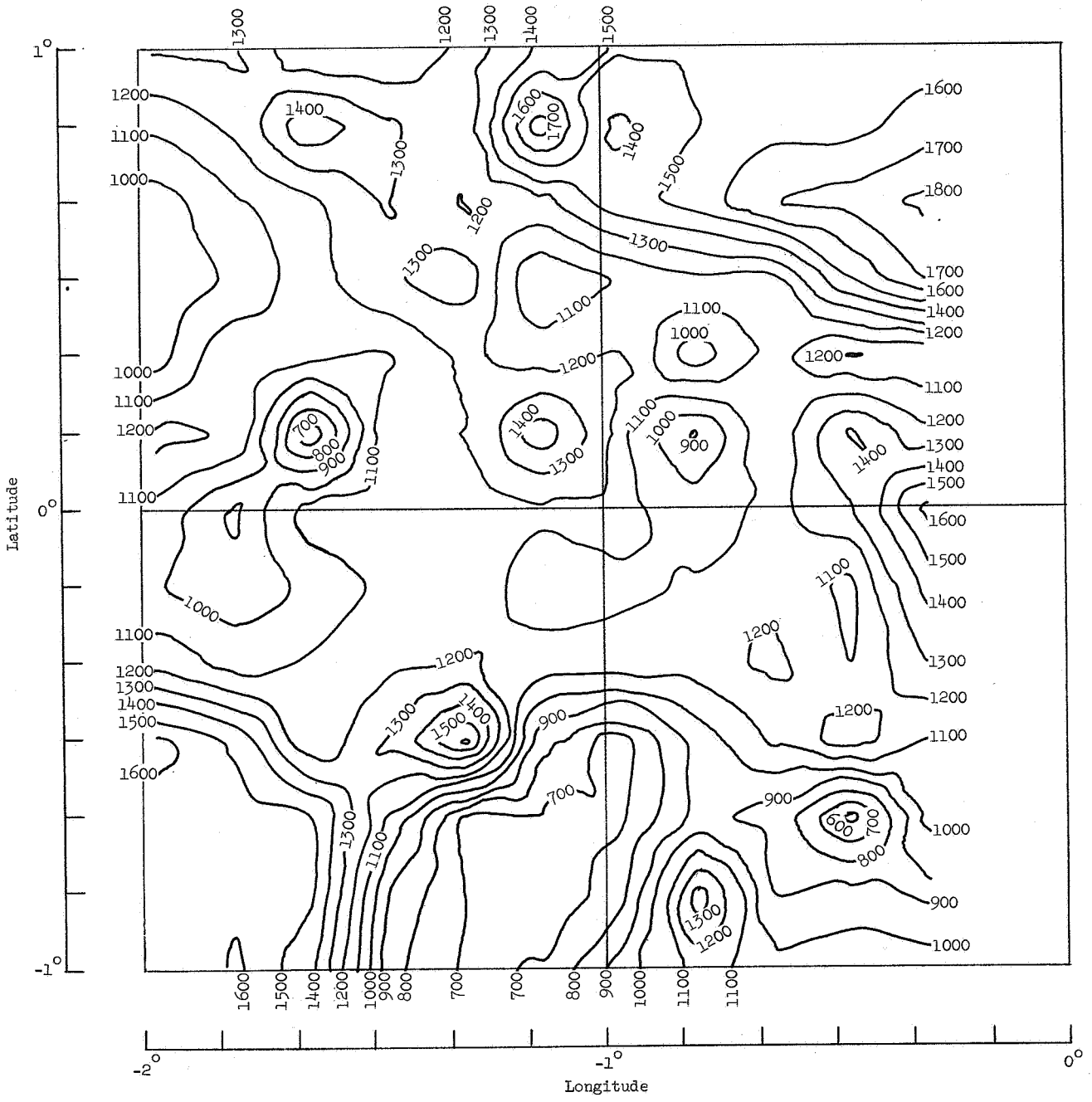

Figure 32.- A computer-generated contour chart of site II P-8BC. Scale: 10 min ≡ 5047 meters.

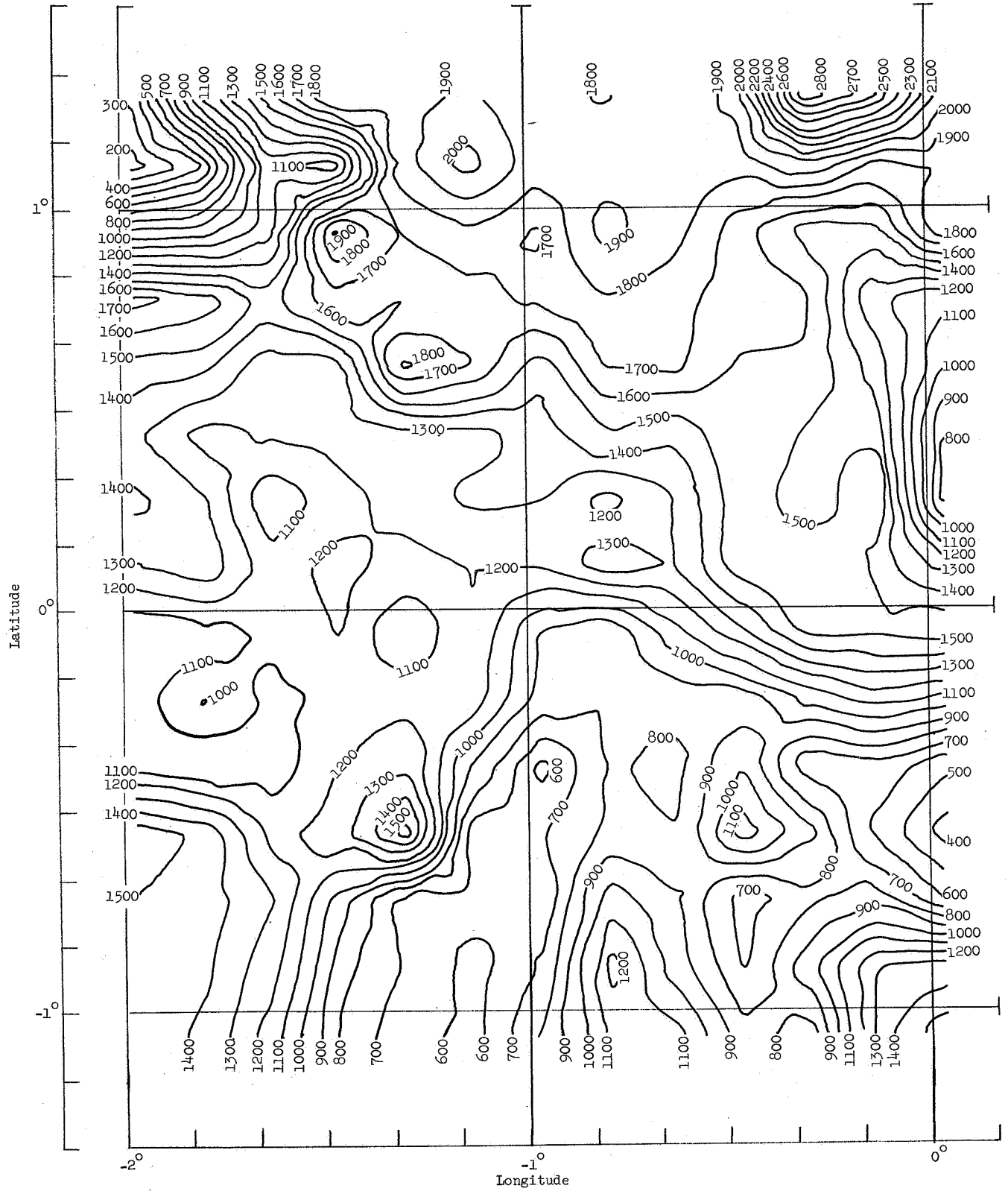

Figure 33.- A computer-generated contour chart of site II P-8AC. Scale: 10 min ≡ 5047 meters.

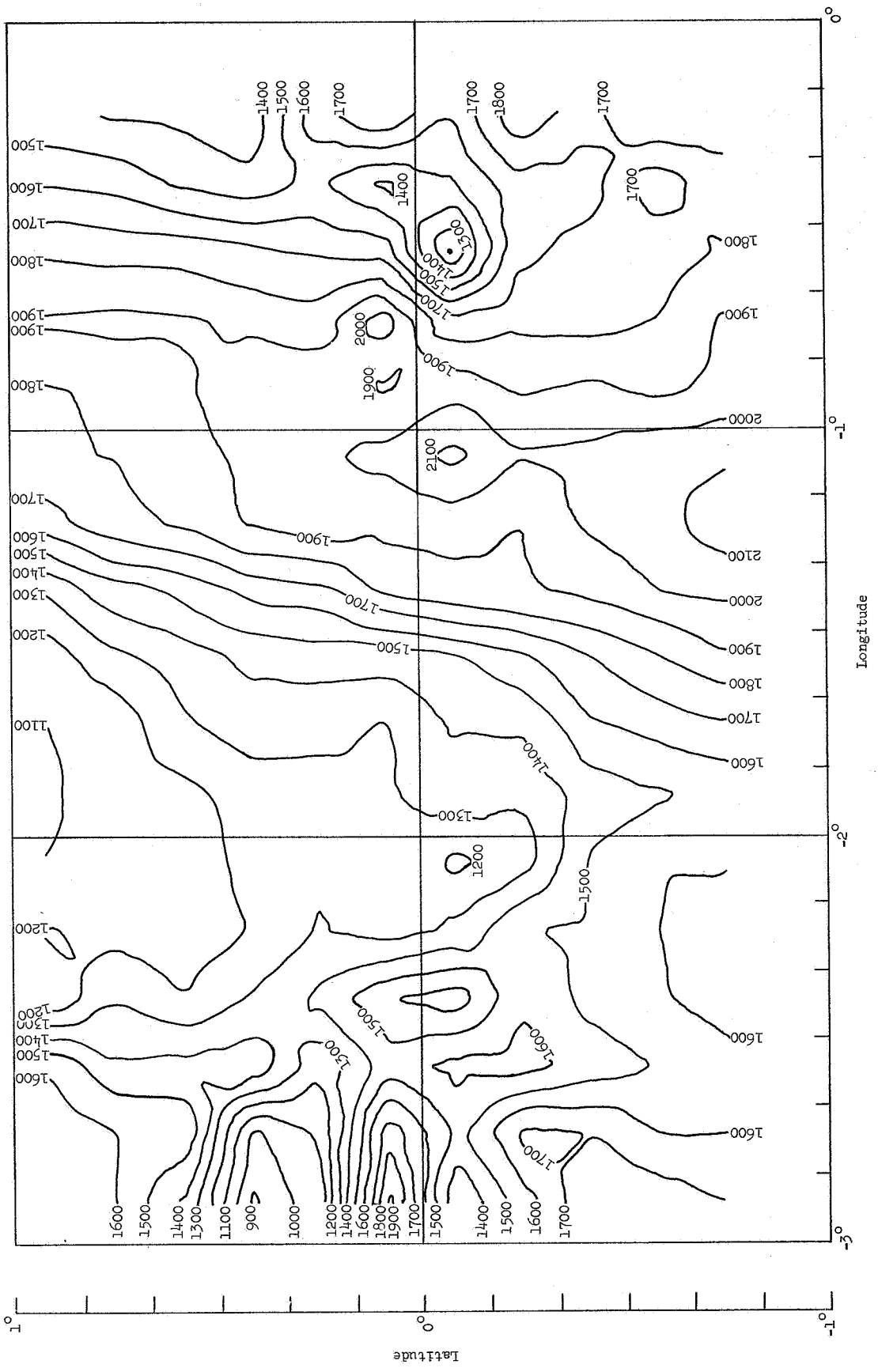

Figure 34.- A computer-generated contour chart of site I P-5. Scale: 10 min = 5047 meters.

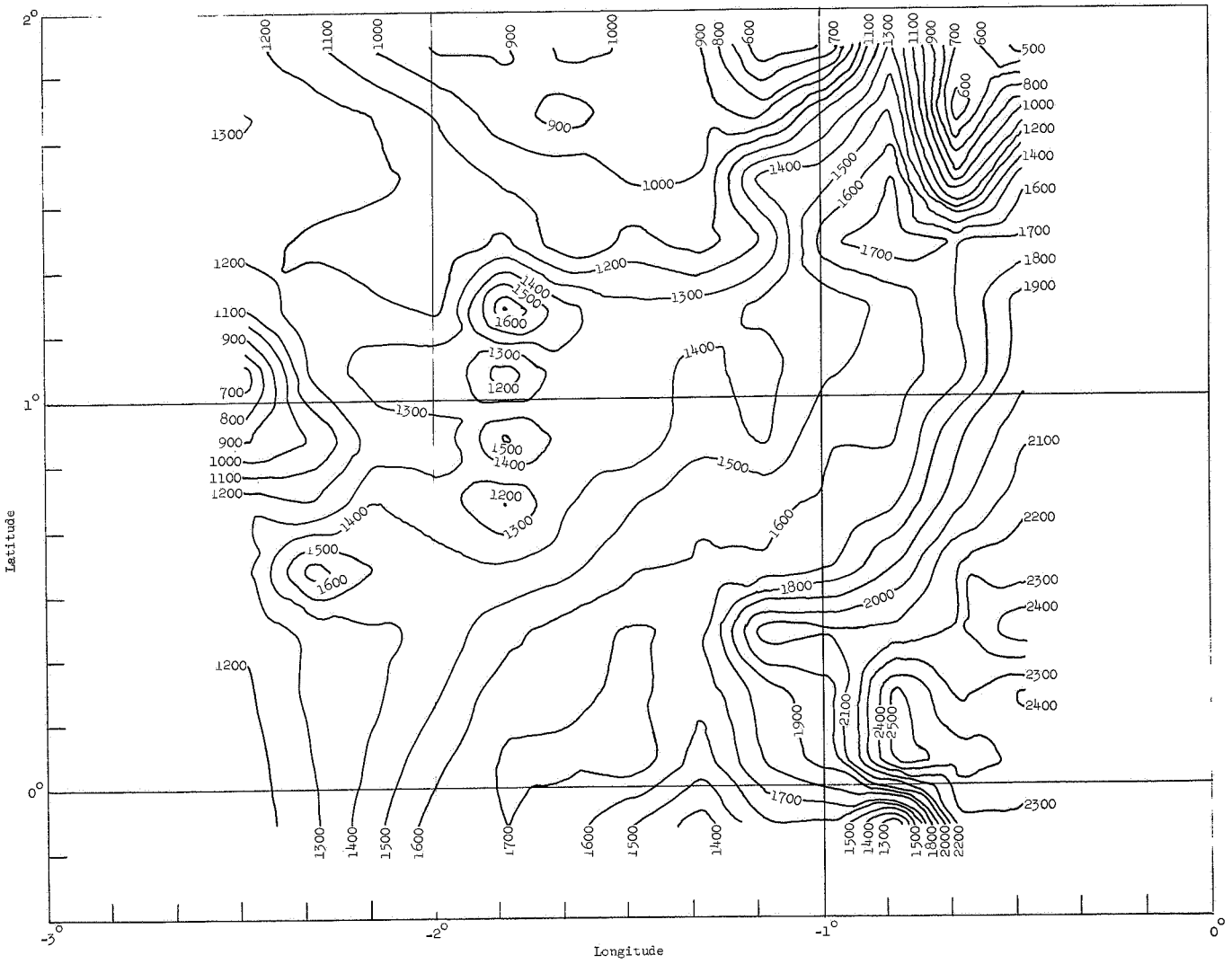

Figure 35.- A computer-generated contour chart of site III P-7AB. Scale: 10 min ≡ 5047 meters.

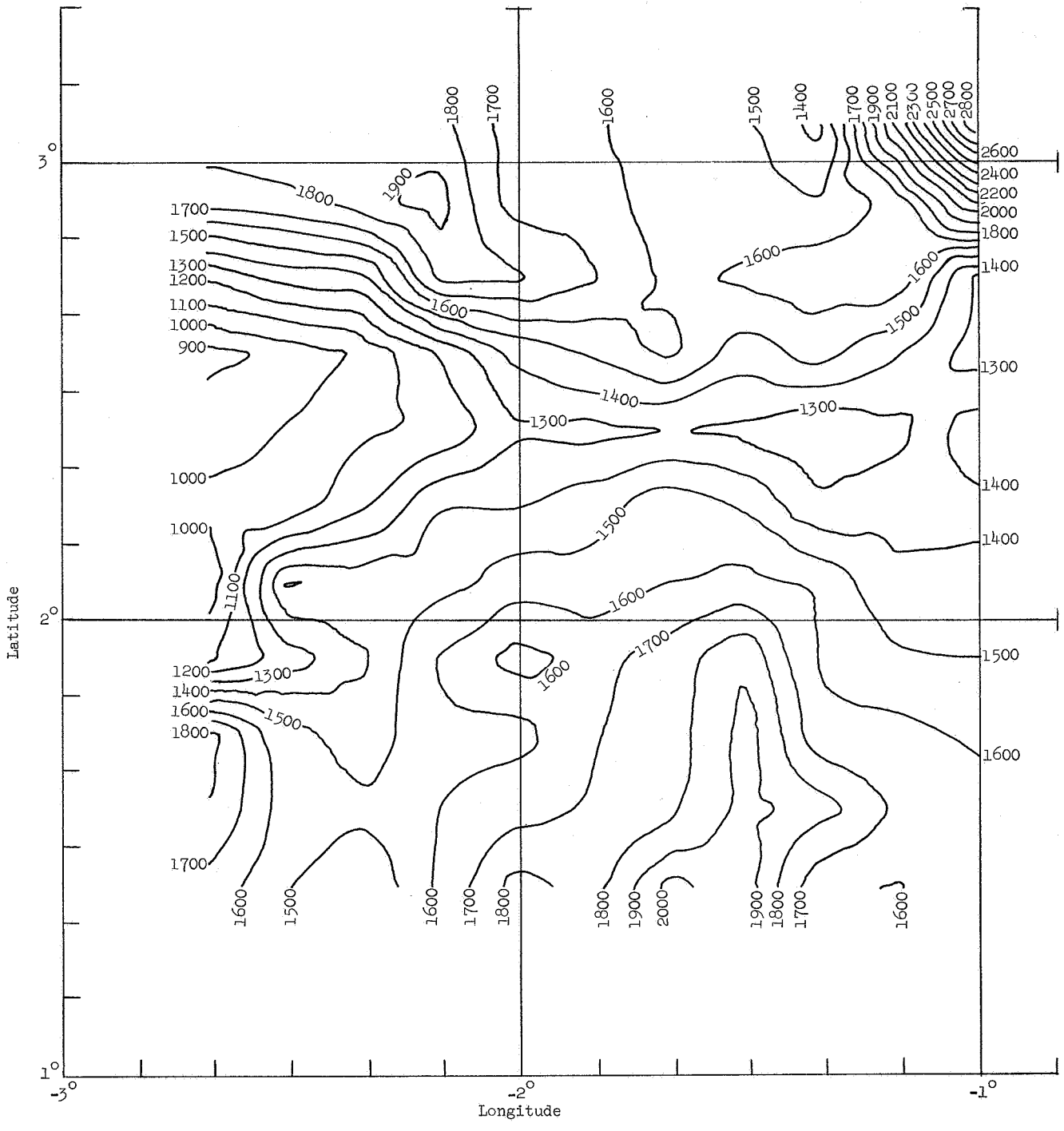

Figure 36.- A computer-generated contour chart of site II P-7AB. Scale: 10 min ≡ 5047 meters.

NASA-Langley, 1970 —— 30 L-6981